FAST NEUTRON DEPTH DOSE DISTRIBUTIONS IN A HETEROGENEOUS PHANTOM

A THESIS

Presented to

The Faculty of the Division of Graduate Studies

by

Joseph J. Shonka

In Partial Fulfillment

of the Requirements for the Degree

Doctor of Philosophy

in the School of Nuclear Engineering

Georgia Institute of Technology

May, 1978

FAST NEUTRON DEPTH DOSE DISTRIBUTIONS IN A HETEROGENEOUS PHANTOM

Approved:

Karl Z. Morgan, Chairman

Joseph D. Clement

Robert H. Fetner

Patton H. McGinley

John W. Poston

Date approved by Chairman: May 31, 1978

ACKNOWLEDGMENTS

The author would like to express his gratitude for the patience and advice of all committee members and advisors. Professor F. W. Chambers, Jr. served as advisor for this dissertation during the early portion of the work. His assistance in the early phases of the work is appreciated. Dr. K. Z. Morgan graciously assumed responsibilities as advisor following Professor Chambers' retirement, and functioned as advisor for the bulk of the dissertation work. Drs. J. W. Poston and J. H. Thorngate served as Laboratory dissertation advisors for that portion of the work done at the Oak Ridge National Laboratory, and their assistance is appreciated. Other members of the reading committee were Drs. G. G. Eichholz, D. S. Harmer, C. J. Roberts and P. H. McGinley. Their advice and suggestions were very much appreciated. Dr. G. G. Eichholz was especially helpful in assisting with the organization of the dissertation itself, and Dr. P. H. McGinley offered considerable technical advice. Mr. T. D. Jones, although not a committee member, offered a good deal of technical advice for the calculational portion of the work.

The author would also like to thank Dr. J. A. Auxier, who along with Dr. Poston rendered assistance in obtaining financial assistance at Oak Ridge. Dr. R. Cloutier from the Oak Ridge Associated Universities and Dr. J. Spokas from the Physical Sciences Laboratory courteously loaned equipment vital to the experimental portion of the work.

This work was performed in part on a Laboratory Fellowship at the

Oak Ridge National Laboratory, and the author is grateful for that aid. A consulting contract with ORNL under Mr. F. F. Haywood also provided support for this work.

The patience and assistance of Lydia S. Geeslin, who typed the document, is gratefully acknowledged, along with her many useful suggestions. In addition, the experimental portion of this work was facilitated by members of the support staff at ORNL including: L. A. Lee, C. P. Littleton, C. Fritz, W. Bunch, and W. Carrothers.

Finally, the support and encouragement of two people proved vital to me. Without the companionship of my wife, D. B. Shonka, and friendship of R. B. Gammage this work might not have been completed.

TABLE OF CONTENTS

TABLE OF CONTENTS (Concluded)

LIST OF TABLES

LIST OF ILLUSTRATIONS

LIST OF ILLUSTRATIONS (Concluded)

SUMMARY

A Monte Carlo code has been developed which can be used to calculate parameters of interest in the Reference Man series of phantoms. The code has been employed in calculations simulating the Rijswijk pre-clinical neutron therapy studies. Results obtained from the code for an A-P exposure of the left lung included the absorbed dose to various organs and the depth dose distribution, neutron spectra, and LET spectra.

The neutron transport was taken from GTC, a code derived from 05R which has been used extensively for depth dose studies. The gamma transport came from ALGAM, a code derived from OGRE which has seen wide application in internal dosimetry problems. Cross sections used in the code were obtained from the GTC cross section library and the ENDF/BIV library. The Reference Man series of phantoms is derived from data in the recently published Reference Man report. These phantoms contain three regions of differing composition and density: lung, skeleton (which is an average of bone and marrow), and the total body less lung and bone (an average of the remaining body organs).

Comparisons have been made with published results from Rijswijk as well as those of McGinley. In addition, measurements made by the author at the Oak Ridge National Laboratory are presented. Experimental measurements were made for four cases: a homogeneous soft tissue phantom and heterogeneous phantoms with soft tissue and lung, soft tissue and skeleton, and soft tissue with lung and skeleton, respectively. These

measurements were made in a physical mockup of the Reference Man phantom using Lucite organs filled with equivalent substitutes for skeleton, lung, and soft tissue. These measurements used a small tissue-equivalent proportional counter, a tissue-equivalent ionization chamber, and an energy compensated G-M tube. From all techniques, total dose, LET, fast neutron dose and gamma dose were derived as a function of depth in the thoracic region.

CHAPTER I

INTRODUCTION

Background

Historical Perspective

In 1937, Stone and his co-workers started the first clinical trials of fast neutrons (Stone and Larkin, 1942). Cyclotron-produced neutrons were used to treat a variety of tumors in 249 patients, all but one of whom were considered incurable by conventional techniques. Many had had prior treatment with surgery, x-rays, and radium therapy. Of the 249, 17 patients survived for periods of time exceeding five years. All of the patients developed severe late skin reactions with ulceration and extensive fibrosis of the treatment area. In the twelfth January Memorial Lecture in 1947, Stone summarized his results: "Neutron therapy as administered by us has resulted in such bad late sequelae in proportion to the few good results that it should not be continued . . .." (Stone, 1948). His warning served as a deterrent of fast neutron therapy for many years, since he interpreted his results as a large relative biological effectiveness (RBE) for late effects.

In December of 1949, a report was made on the formation of cataracts in cyclotron physicists (Abelson and Kruger, 1949). Ten researchers were found to have cataracts. The average dose to the lens of their eyes was approximately 120 rads, with the neutron exposures occurring as long as

ten years prior to the study. This verified the high RBE values for late effects reported by Stone.

During the next decade, slow neutron capture therapy was unsuccessfully tried at two installations in the United States (Fowler, 1964). Severe skin effects were noticed at dose levels far below tumoricidal doses. Necrosis occurred even when the skin was cut and turned back from the beam and replaced following irradiation. This was attributed to diffusion of the thermal neutrons coupled with a high RBE of the neutrons.

Recent biological evidence, combined with Stone's complete documentation of his early trials, has shown that the late effects from fast neutron irradiation were due to an underestimation of the dose equivalent. The early workers had measured the RBE of neutrons for a single dose, but the treatment was administered in fractions. In addition, the schedule of fractions could not be met reliably because of the erratic machine output. It is now known that RBE for fast neutrons increases rapidly at low doses (less than 100 rads) and increases with decreasing neutron energy (Fowler and Morgan, 1963).

The fact that RBE increases rapidly as the dose is decreased has recently received renewed attention. In radiation protection a quality factor of 10 for fast neutrons is commonly assumed independent of the total dose. This quality factor is meant to be a conservative estimate of maximum RBE. In reexamining the data on survivors of Hiroshima and Nagasaki, Rossi and Mays have determined that the RBE for fission neutrons in producing leukemia could be as high as 72 at a dose level of one rad (Mays, 1977). These data are estimated to be uncertain to a factor of two and

were derived from the fact that Hiroshima survivors had a biologically significant neutron dose while the Nagasaki weapon resulted primarily in gamma exposure (Mays, 1977).

This recent work by Rossi and Mays will undoubtedly require reevaluation of quality factor and the concept of RBE. RBE is defined as the ratio of the dose of gamma radiation (usually ^{60}Co or filtered 250 kVp x-rays) to the neutron dose required to produce the same effect. Repair mechanisms have been demonstrated for photon radiation and a number of studies have indicated that the effect per rad for high LET radiation is greater at low dose than at high dose; both of these trends would tend to increase RBE.

Rationale Behind Neutron Therapy

As biological evidence accumulated during the 1950's, researchers began to comprehend the reason for the failure of the Stone fast neutron therapy trials. Following a thorough set of experiments, a new trial was initiated in 1967 at the Hammersmith Hospital in London (Catterall, 1971). By 1971, results were encouraging enough that a randomized prospective trial was started, in which preliminary results have been satisfactory (Catterall, 1974). There are several reasons why new fast neutron trials have been attempted even after Stone's admonition.

The cells in the interior of solid tumors tend to have lower oxygen tension than the exterior and surrounding tissue cells due to poorer vascularization and great oxygen demand of the rapidly dividing tumor cells at the periphery. These hypoxic cells require two to three times the x- or gamma-radiation as oxygenated cells for the same degree of killing.

This is known in radiobiology as the oxygen effect. Fast neutrons have a greater specific ionization or greater average LET than electrons or x-rays and exhibit a much smaller oxygen effect. In modern radiotherapy, the dose that one can deliver to the tumor is limited by its effect on the normal tissue surrounding it. The decreased sensitivity of the hypoxic tumor cells to low LET radiation may permit some fraction of those in the interior of the tumor to survive and regenerate at dose levels where the surrounding tumor cells have been eliminated and normal tissue has been seriously damaged. If surviving tumor cells regenerate the tumor, a local failure to cure has occurred. Radiation, such as neutrons, with higher average LET and a concurrent much smaller oxygen effect, might improve the local cure rate in hypoxic tumors (Fry, et al., 1972). This could have a significant impact on the overall cancer death rate as death of cancer victims due to failure of radiation therapy currently claims nearly 100,000 lives each year in the United States, or roughly one quarter of all cancer deaths in the United States (Powers, 1972).

Rijswijk Therapy Studies

The Hammersmith trials used a spectrum of neutrons produced by bombarding a beryllium target with cyclotron accelerated deuterons. This arrangement is inconvenient compared with modern therapy machines which provide rotational fields and flexible patient positioning. The deuterium-tritium reaction produces isotropic high-energy neutrons at low accelerator energies. If target lifetime problems can be solved, this reaction produced by a small accelerator might be the ideal source for neutron therapy. Radiation biologists at the Radiobiological Institute in the

town of Rijswijk in the Netherlands, initiated a program aimed at evaluating radiation biology parameters fundamental to neutron therapy with an eventual clinical trial using (D,T) neutrons as the ultimate goal.

At an advanced stage, a malignant tumor often metastasizes, or spreads to other parts of the body. A frequent location for metastasis is the lung, where faced with a virtually unlimited blood and oxygen supply, and low density tissue, a tumor will grow rapidly. At this stage, palliative radiation therapy is frequently employed to shrink tumors in the lung to ease suffering and make breathing less difficult. Researchers at Rijswijk collimated (D,T) neutrons so that they impinged on one lung. In a given patient, one lung was treated with ^{60}Co gamma radiation while the other was treated with 14 MeV neutrons during one fraction of the therapy schedule. Radiographs before and after treatment allowed comparison of tumor response (as measured by shrinkage of similar tumors in both lungs) for conventional and neutron therapy. This information was then used to derive RBE values for various tumors under oxygenated conditions (Barendsen, et al., 1974).

Objectives of Dissertation

With the growing interest in neutron therapy there is need for a reliable Monte Carlo code which could be used to calculate parameters of interest in a realistic phantom. With this in mind, two broad objectives can be stated for this dissertation:

1. Develop a transport code capable of describing the transport of photons and neutrons in a heterogeneous phantom. The code should calculate parameters such as dose from neutrons, dose from photons, and dose as a function of LET.

2. Develop dosimetry techniques to test the code for 14 MeV neutrons, a neutron energy of interest to therapy. A comparison of experimental results with a geometry identical to that of the code, as well as with similar geometries whose results are in the literature, would supply a test for the code.

Interactions of Radiation with Tissue

Composition of Tissue

When one considers the interactions of any penetrating radiation with matter, a knowledge of the composition of that matter is of prime importance. The number and type of atoms and the density of the medium are required to calculate transmission and energy deposition in matter. Mindful of these requirements, workers in radiation dosimetry have considered this problem over the years. This has resulted in a series of publications of increasing sophistication, the latest of which was published in 1975, the Reference Man (ICRP, 1975). This report lists anatomical and physiological data along with elemental data for a "reference man," and forms the basis for many estimates of maximum permissible limits for radiation exposure. These data also formed the basis of a calculational model used extensively in internal dose estimates. Since the Reference Man is the best available compilation on the average composition of tissue, its values were used for this dissertation. A computer model based on Reference Man was developed in the late 1960's by Snyder et al. (Snyder et al., 1968). Three compositions which represent the greatest diversity of human tissue were selected--for skeleton, lung, and

tissue, respectively. The compositions and densities are shown in Table 1. Skeleton is an average of approximately 7000 grams of bone tissue with 3000 grams of red and yellow marrow. The tissue composition was derived by subtracting skeleton and lung values from the totals in the Reference Man.

Heavy Charged Particle Interactions with Tissue

Neutron reactions produce heavy charged-particle recoils in tissues when they undergo scattering collisions. These charged particles are the high-LET radiation responsible for most of the dose and most of the damage to cells accompanying neutron irradiation of tissue. A theoretical discussion of the processes contributing to stopping power of heavy charged particles generally considers stopping in four energy ranges: low, intermediate, high, and very high.

At very high incident ion energies, nuclear interactions predominate. These processes are analogous to high energy neutron interactions and result in absorption of the incident particles and emission of decay products. The cross section for the various reactions is a function of the energy of the particle. For protons, these reactions begin to become significant at energies greater than 100 MeV. For example, a 60 MeV proton has a mean free path for nuclear interactions of 70 g/cm^2 in aluminum. The range in aluminum due to electronic stopping is approximately 7 g/cm^2. Thus electronic stopping is the dominant mode of energy deposition. At higher energies, the reverse is true, and both stopping power and range no longer characterize the particle (Bichsel, 1968).

At high energies, the ion can be considered to be fully ionized.

Table 1. Composition of the Three Media Selected to Represent the Human Body (Percent by Weight)

Element	Skeleton	Lung	Tissue
H	7.04%	10.2	10.5
C	22.8	10.0	23.0
N	3.86	2.80	2.34
O	48.6	76.0	63.2
Mg	0.11	0.007	0.02
P	6.94	0.08	0.24
S	0.17	0.23	0.22
Ca	9.91	0.007	0
Cl	0.14	0.27	0.14
K	0.15	0.20	0.21
Na	0.32	0.19	0.13
Density (g/cc)	1.5	0.3	1.0

For a proton, this region corresponds to energies between 1 and 100 MeV. The classical theory of Bohr was first used to explain stopping in this region and was later generalized by Bethe who derived the quantum mechanical expression:

$$S = \frac{4\pi Z^2 e^4}{M_e V^2} \cdot \frac{N_0 \rho}{A} \cdot Z' \cdot \left\{ \ln \frac{2 M_e V^2}{I} - \ln(1-\beta^2) - \beta^2 \right\} \quad (1)$$

where

Ze = charge of ion

Z' = atomic number of medium

V = velocity of ion

$N_0\rho/A$ = atoms per cc of medium

M_e = electron mass

I = ionization potential of media.

Two corrections to this formula are generally used in a computation of stopping power. One is called the shell correction, first employed by Walske. It reduces stopping by a factor to account for the fact that inner shell electrons have velocities comparable to the velocity of light, where the original theory assumes the velocity of the ion is much greater than that of the electron. The second correction is called the density effect. This reduces stopping power of ions in the nonrelativistic range of energies, and is due to the fact that polarization of the media established by the charge of the ion shields distant atoms in the media, thus reducing the stopping power.

At intermediate ion energies (10-800 keV for a proton) the net charge of an ion is reduced by capture and loss of electrons as the

ion moves through the medium. The Bethe stopping power equation, with shell and density corrections, is valid, but the charge of the particle is reduced by a quantity related to the velocity of the particle. Barkas (1963) derived the expression which described the loss of effective charge by the ion:

$$Z^* = \left[1 - \exp\left(-125\,\beta\, Z^{-2/3}\right)\right] \qquad (2)$$

At lower ion energies, electronic (Coulomb) interactions with nuclei become important. Lindhard et al. (1963) derived an expression for nuclear Coulomb stopping. This contribution to stopping power is added to the electronic stopping power for the total stopping. In the Lindhard theory, Bethe's equation for electronic stopping is often replaced with the simpler expression:

$$S = k\sqrt{E} \qquad (3)$$

Photon Interactions with Tissue

Photons are produced in tissue any time that tissue is irradiated by neutrons. Moreover, all neutron sources currently used for therapy have some photon contamination.* Four processes dominate the interactions these photons undergo in tissue: pair production, Compton scattering, photoelectric absorption, and Rayleigh scattering.

Pair production is an event which absorbs the photon. In the intense electric fields near a nucleus, the photon can be absorbed with the emission of a positron-electron pair. This requires the photon to have a

*It should also be noted that high energy x-ray sources may produce neutrons.

minimum or threshold energy equal to the rest mass of the two particles, viz. 1.02 MeV. Almost all of the photon energy above the threshold appears as kinetic energy shared by the positron-electron pair. The cross section for pair production varies with photon energy and Z^2/A of the medium. As the positron slows, it will annihilate with an electron producing two quanta of 0.511 MeV each.

Compton scattering is a process where a photon interacts with an orbital electron. The electron can acquire any energy from zero to a maximum given by the expression:

$$E_{max} = h\nu_o \frac{2\alpha}{1+2\alpha} \qquad (4)$$

where

$h\nu_o$ = the incident photon energy

α = ratio of photon energy to the rest mass of an electron ($m_o c^2$).

The cross section for Compton events varies as Z/A. This ratio is approximately equal to one half for elements other than hydrogen, where Z/A equals one. At photon energies greater than the rest mass energy of an electron, the cross section for Compton scattering is inversely proportional to the photon energy.

The photoelectric effect occurs when an atom absorbs the entire photon and ejects an electron with an energy equal to the difference of the photon energy and binding energy of the electron. The binding energy appears as characteristic x-rays and Auger electrons. The atomic cross

section for the photoelectric process is proportional to Z^5/A and is inversely proportional to the photon energy cubed.

Rayleigh scattering (also called coherent scattering) is a scattering of the photon by the atom as a whole. Functionally, the process is analogous to Compton scattering; since the mass of the atom is much greater than an electron mass, energy loss and also the scattering angle of the photon tend to be much smaller than in the Compton effect.

Neutron Interactions with Tissue

Because a neutron is uncharged, it will interact strongly only with nuclei in any medium. Five main classes of interaction can occur: capture, elastic and inelastic scattering, nonelastic reactions, and spallation (Auxier, Snyder, and Jones, 1968).

At low neutron energies, capture processes dominate those neutron interactions in tissue that produce significant quantities of dose. In human size masses of soft tissue, two capture reactions predominate: $^{1}H(n,\gamma)^{2}H$ and $^{14}N(n,p)^{14}C$. Lung has nearly the same composition as soft tissue, and thus the same capture reactions dominate. Most other capture reactions of interest have macroscopic cross sections at least two orders of magnitude smaller. Thus their importance is small as measured by contribution to total dose from neutrons. However, other reactions are noteworthy. The sodium capture reaction, $^{23}Na(n,\gamma)^{24}Na$, is important in health physics since the lifetime of the ^{24}Na (14.96 hr) lends itself to a convenient system for evaluating an accidental exposure to neutrons. Skeletal tissue differs enough from soft tissue that other reactions can contribute to the thermal neutron dose.

The research described in this dissertation utilized the mathemati-

cal model developed by Snyder et al. (1968). In that work, raw bone (roughly 7000 g for Reference Man) was averaged with red and yellow marrow (roughly 1500 g each). This resulted in nominal skeletal tissue intermediate between soft tissue or bone. In this tissue, as in soft tissue, hydrogen and nitrogen capture reactions predominate. The macroscopic cross sections for other reactions begin to approach 10-20% of the nitrogen capture cross section. Among these, capture reactions with phosphorus, calcium, and chlorine are of particular importance.

At neutron energies up to at least 15 MeV, elastic scattering with hydrogen dominates both in terms of interactions and dose deposited. Figures 1, 2, and 3 show the importance of various elements in soft tissue, lung, and bone. The total kerma factor* at a given energy was divided into the kerma factor contribution for each element. The values of kerma factor for the elements were taken from the recent Neutron Dosimetry for Biology and Medicine (ICRU, 1977). Figure 1 shows that, for soft tissue, interactions with hydrogen dominate the kerma to at least 30 MeV. At 15 MeV 70% of the kerma is contributed by interactions with hydrogen; oxygen and carbon interactions contribute 19% and 9.5%, respectively. Nitrogen interactions contribute no more than 1% to the kerma at energies approaching 20 MeV. All other elements never contribute more than 0.05% at energies below 30 MeV. Figure 2 shows that, for lung tissue, the situation is very similar. The only noticeable change is that oxygen becomes slightly more important and carbon slightly less important as would be expected from the concentrations shown in Table 1. This effect is not due

*Kerma factor is the quotient of kerma by fluence, also called fluence-to-kerma factor.

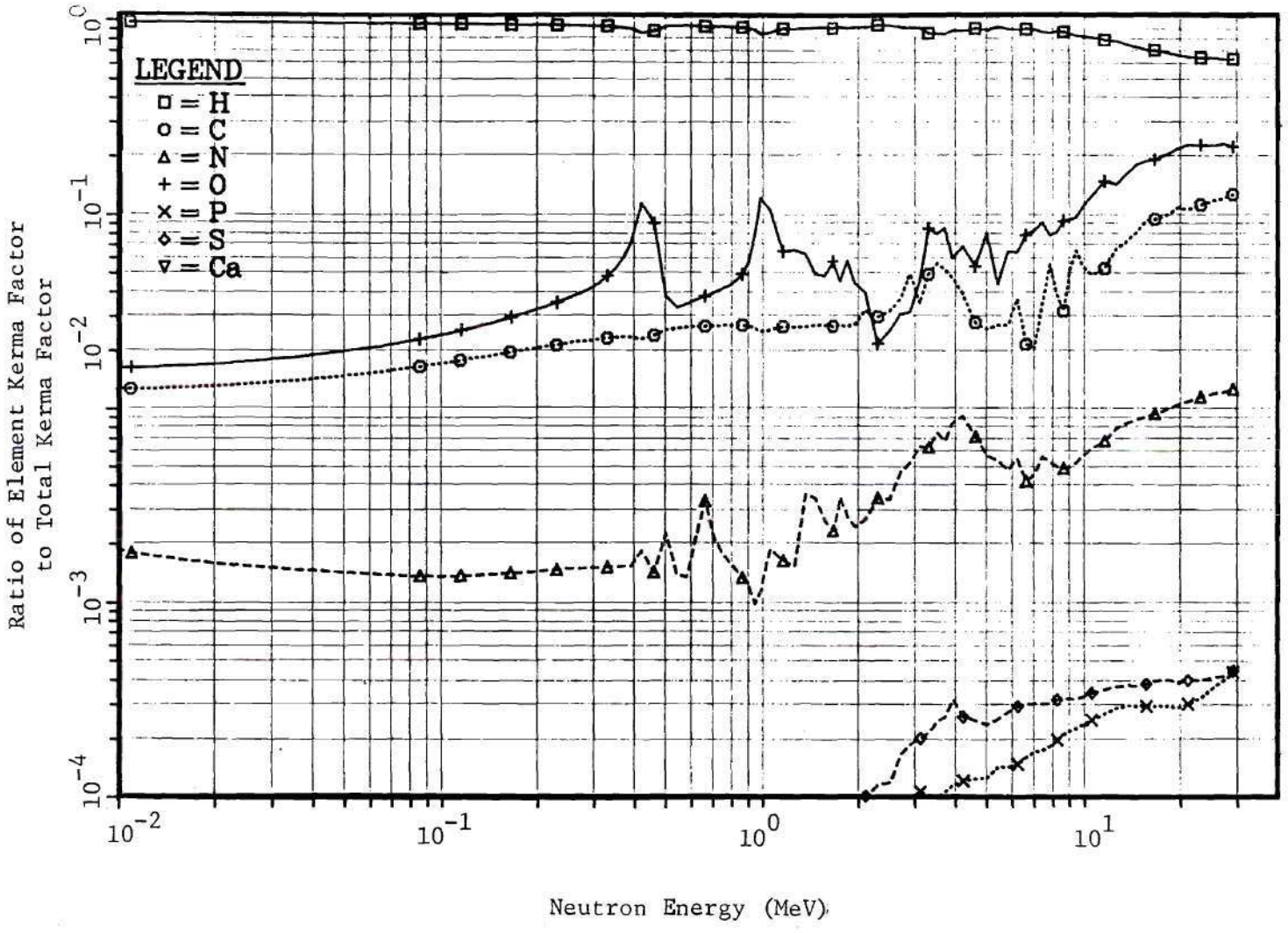

Figure 1. Contribution to Kerma as a Function of Energy and of Element in Soft Tissue

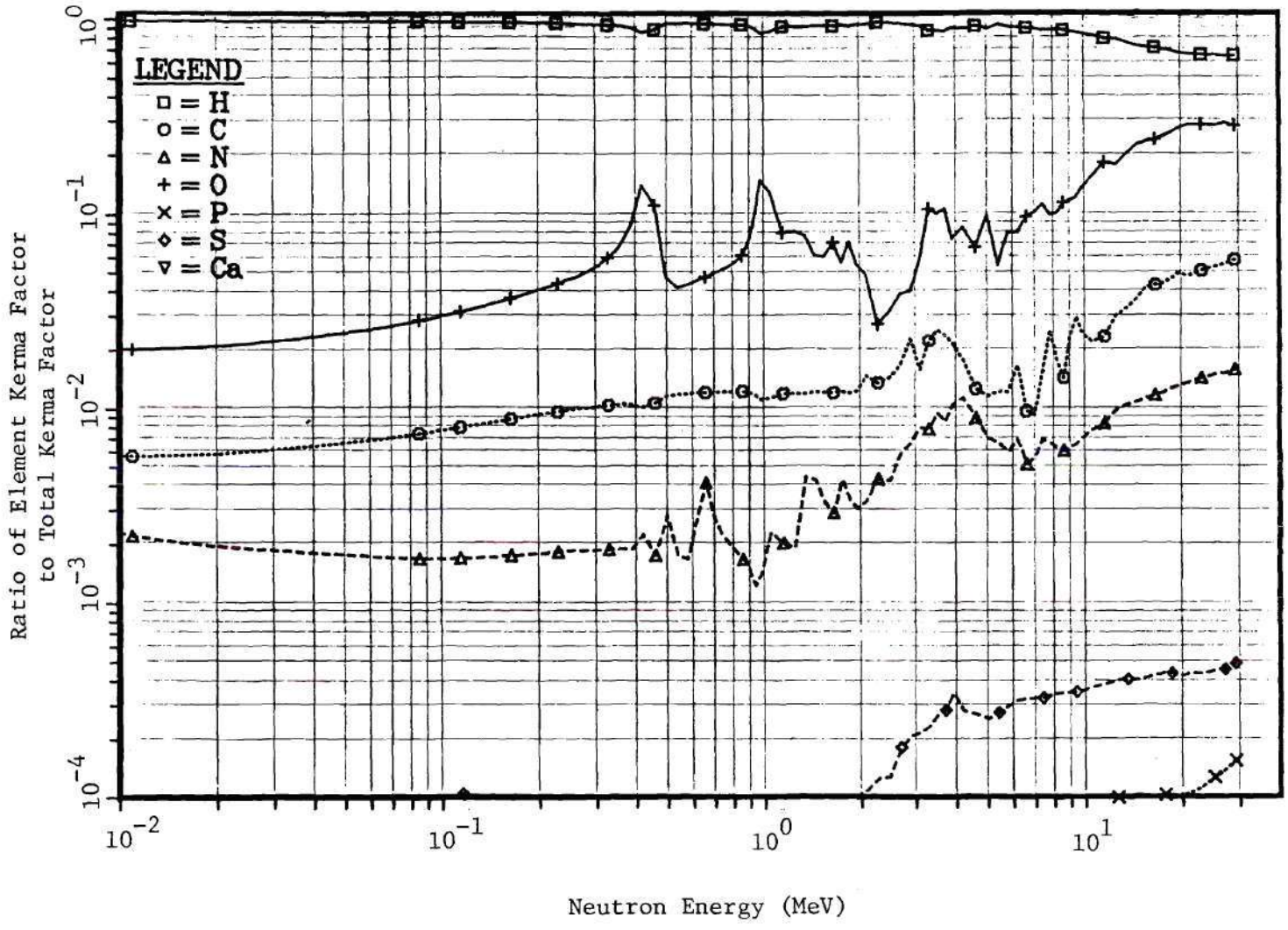

Figure 2. Contribution to Kerma as a Function of Energy and of Element in Lung

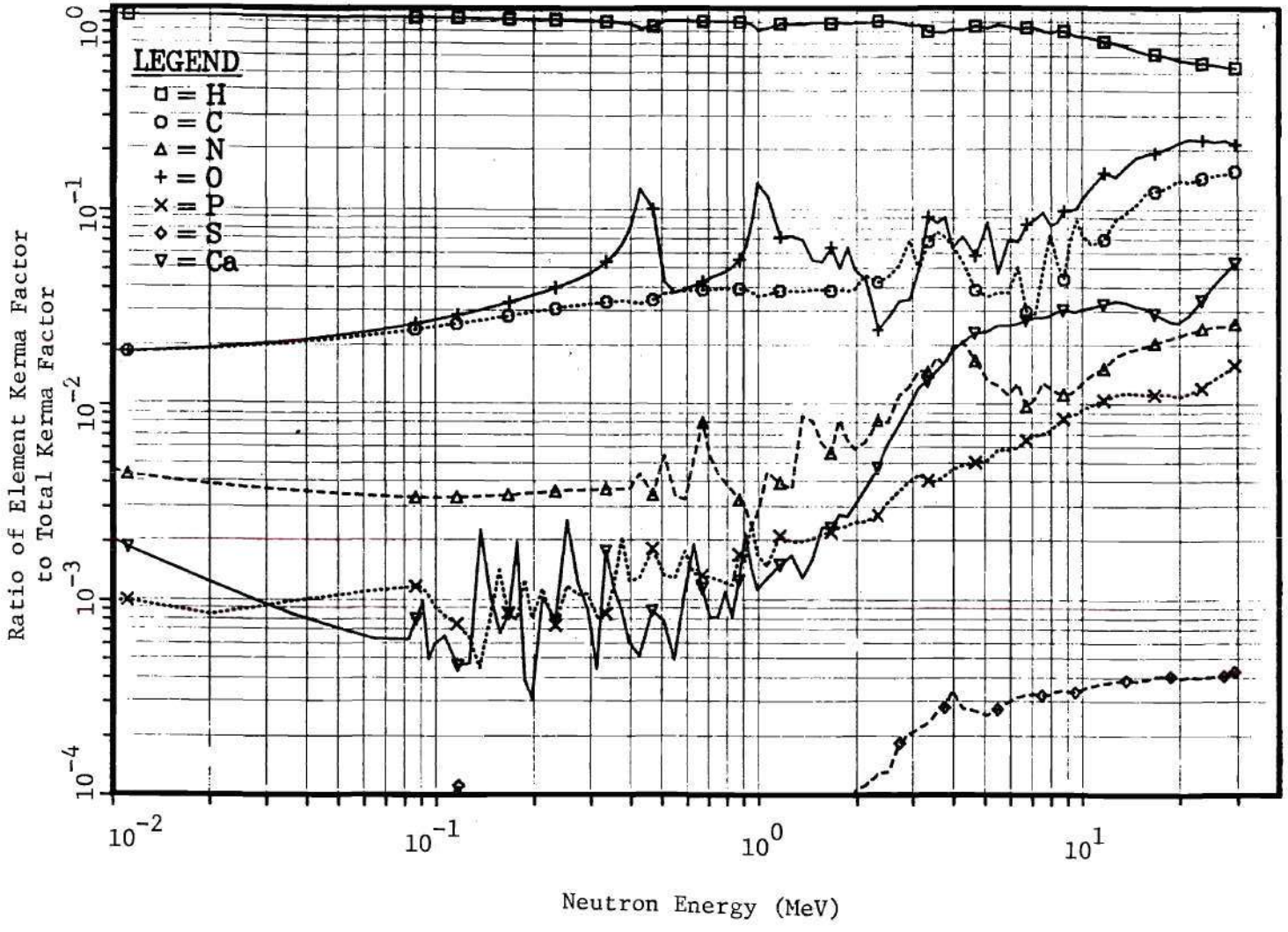

Figure 3. Contribution to Kerma as a Function of Energy and of Element in Skeleton

to air in the lungs, since nitrogen would have to experience an even greater increase which it does not. This insignificant contribution by air is reasonable since air is approximately 0.1% the density of tissue.

Figure 3 shows that, in the case of skeletal tissue, two other elements, calcium and phosphorus, become as significant as nitrogen in their contributions to kerma. This appears to occur at the expense of hydrogen.

All three of these graphs were computed from kerma averaged over rather broad energy bands. This averaging process suppresses much, but not all, of the fine structure that cross sections exhibit in resonance regions.

The total kerma factor is given in Figure 4 for the three types of tissue and it is computed from data in the same source (ICRU, 1977).* The smooth appearance of these curves for the three media reflects the dominance of hydrogen elastic scattering. Small irregularities on the otherwise smooth curves can generally be traced to a resonance in the cross section of one of the other elements, most often oxygen. These discontinuities in what would otherwise be a smooth function of energy do not significantly change the dose computed by a Monte Carlo code since averaging occurs in the calculation. As shown in Figure 4, kerma factor in lung and soft tissue is nearly identical. Skeletal tissue kerma factor does differ, but the difference remains similar over a wide range of energies so that the curves almost parallel each other. It is interesting

*On this graph and subsequent ones, the word tissue refers to soft tissue. Unless otherwise stated, the word tissue in the text also refers to soft tissue.

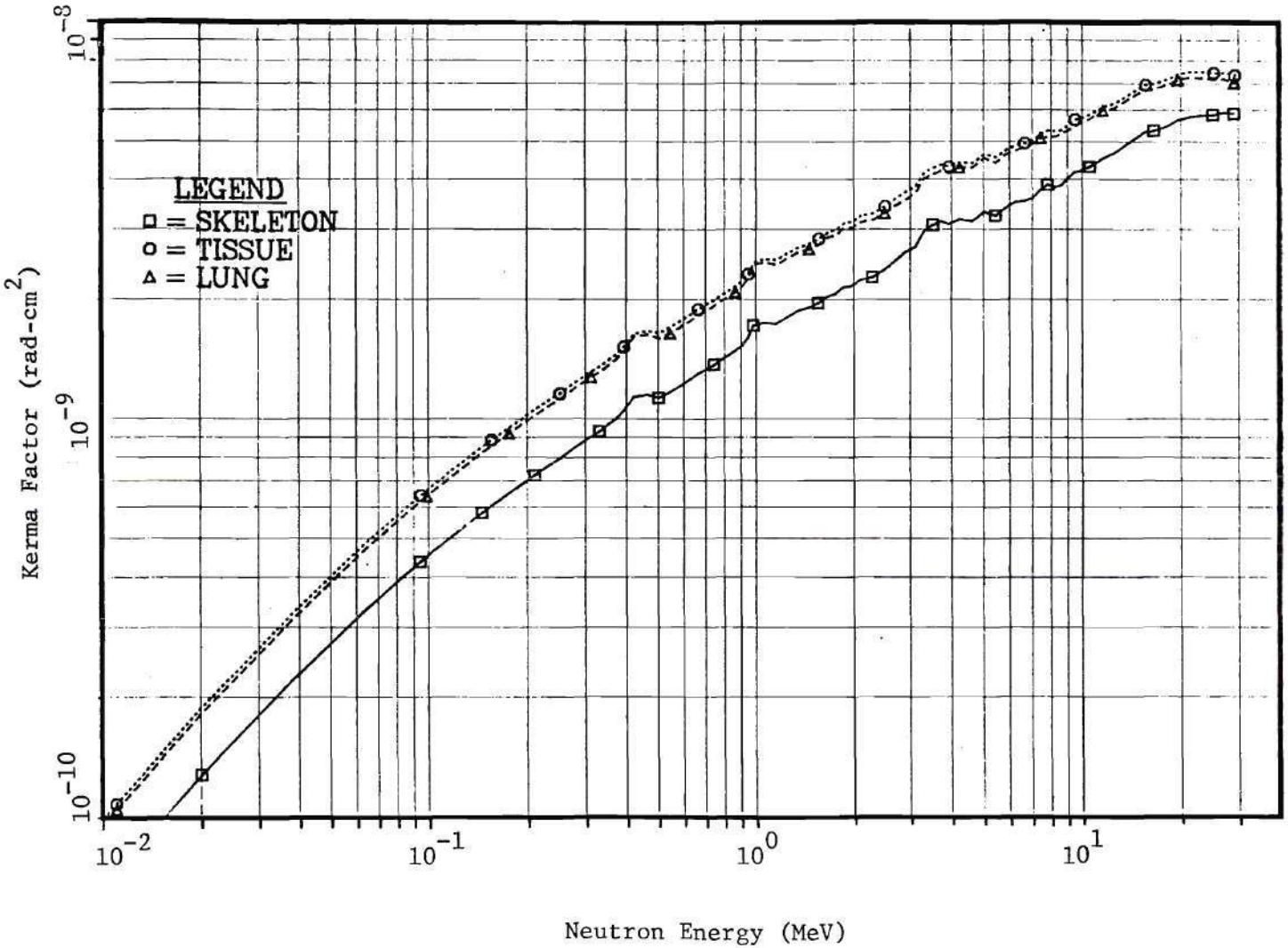

Figure 4. Kerma for the Three Media in Reference Man

to observe that since the density of skeletal tissue (1.5) is greater than that of soft tissue ($\rho \approx 1$) and the ratio of the values for soft tissue or lung vs skeleton is 1.5 in Figure 4, the total energy deposited in tissue and skeletal tissue is nearly the same. The differences in the previous three graphs reflected the abundance of the various elements. Except for hydrogen, kerma factors for most light elements are approximately equal. In skeletal tissue, hydrogen is lower as a percent by weight. With the increased density, however, the atoms of hydrogen per cubic centimeter are nearly equal between bone and soft tissue. This results in very similar energy deposition per se.

Monte Carlo Theory and Application

Transport Theory

A precise knowledge of the energy fluence at all points in space allows the calculation of any parameter of interest such as the neutron dose. An exact formulation of the problem is contained in the steady-state Boltzmann equation, which is stated below for a single type of radiation (Fitzgerald et al., 1967):

$$\nabla \cdot \hat{\Omega} N(\vec{r}, E, \hat{\Omega}) + \Sigma \cdot N(\vec{r}, E, \hat{\Omega}) = \iint N(\vec{r}, E', \hat{\Omega}') \eta \sigma_s (\hat{\Omega}' \cdot \hat{\Omega}, E' \to E)\, dE'\, d\Omega' + S(\vec{r}, E, \hat{\Omega}) \tag{5}$$

In this notation

Σ = total macroscopic cross section; (cm^{-1})

η = number of nuclei per cc; $= N_0 \rho / A$

σ_s = differential scattering cross section for particle of energy $E' \to E$, and direction $\hat{\Omega}' \to \Omega$ (cm^2/atom)

$S(\vec{r}, E, \hat{\Omega})$ = source term, the number of new particles produced per unit time with energy E, direction $\hat{\Omega}$.

$N(\vec{r}, E, \hat{\Omega})$ = the angular fluence, the number of particles per unit volume at r; per unit solid angle, per unit energy, per unit time with energy E, direction $\hat{\Omega}$.

Equation (5) is a statement of the conservation of neutrons in a six-dimensional phase space. There are three spatial coordinates, an energy coordinate, and finally two coordinates specifying direction. The left hand side of equation (5) expresses the loss of neutrons. The first term is the loss of neutrons due to leakage out of the volume. The second term is the loss of neutrons by absorption and scattering. The right hand side represents the increase in neutrons, the first term being the gain due to scattering into $N(\vec{r},E,\hat{\Omega})$ and the second term being the source term for neutrons generated in N. The Boltzmann transport equation does not lend itself to an analytic solution for any practical problem, although there are two noteworthy methods, the Neumann series and the iteration method, either of which can be used for simple geometry. Approximate solutions can be arrived at using approximations with iteration to a solution, or the elimination of several of the variables. Almost all solutions of non-trivial problems have used one of the following methods: kernel theory, removal-diffusion theory, moments method, spherical harmonics, discrete ordinates, Fermi age theory, or Monte Carlo techniques (Wilkie, 1970). Of all of these, Monte Carlo is the method commonly employed for the calculation of dosimetry problems with complex geometry.

Monte Carlo is a sophisticated technique in which histories are

computed for a large number of neutrons. If the way in which these histories are calculated is unbiased (random), then for a large number of histories one would get an unbiased sample of all possible neutron histories. However, if one merely computed histories from the probabilities of interaction, this technique would not be extremely useful. This is easily seen by the fact that, if one allows S initial neutrons to impinge on a semi-infinite slab of thickness d, and S' penetrate the slab, the transmission is defined as (Goldstein, 1959):

$$F_N(x) = S'/S \tag{6}$$

and has a probable fractional error of

$$0.6745\sqrt{(1-F_N)/F_N \cdot S} \tag{7}$$

which for large values of d becomes:

$$0.6745/\sqrt{S'} \tag{8}$$

Thus one can see that, for 10% accuracy in F_N, S' must be greater than 100. If a thick slab attenuates the neutrons a factor of 10^3, 10% accuracy would require 10^6 primary neutron histories to be traced, a non-trivial task for a computer. Because of this, Monte Carlo techniques require some biasing of favorable (deep penetration) histories to improve accuracy for a fixed number of primary neutrons. Many techniques have

been developed for biasing. Among the more common are: importance sampling, expected values, Russian roulette, splitting, and systematic sampling. In Russian roulette, for instance, the statistical variance is reduced in the following manner: A neutron is given a statistical weight which is unity at the point of origin. At each collision site its statistical weight is reduced by the non-absorption probability. When the statistical weight of the neutron drops below a given value, a game of chance is played where the weight is either doubled or set to zero, depending on the fate chosen by a random number generator. The neutron history continues until terminated by Russian roulette or escape from the region of interest.

Monte Carlo techniques allow calculation of the fluence at any point of interest for a given geometry. In a calculation of depth dose, a large computer is used to record types and locations of interactions.

CHAPTER II

PREVIOUS WORK

Monte Carlo Calculations

Fast neutron fluence-to-kerma factors have been calculated for standard tissue compositions by various authors since the need for them was recognized. One of the early efforts was a calculation by Snyder and Neufeld in 1955. In that work, which two years later was incorporated into NBS Handbook 63, tissue was assumed to be composed of only the four major elements: hydrogen, oxygen, carbon and nitrogen. Elastic isotropic scattering and capture by hydrogen and nitrogen were the only reactions considered. In addition to calculating kerma, results of Monte Carlo depth dose calculations in a 30 cm slab of tissue were presented at six energies from thermal to 10 MeV (Snyder and Neufeld, 1955). The National Bureau of Standards issued revised calculations in Handbook 85, which took into account anisotropic elastic scattering and inelastic scattering (NBS, 1964).

During the next decade, several groups improved on these early kerma calculations by considering nonelastic events which produce charged particles (Auxier, Snyder, and Jones, 1968), (Williamson and Mitacek, 1967), (Bach and Caswell, 1968), and by consideration of additional elements (Ritts et al., 1971). The lack of adequate cross section information precluded detailed treatment of these factors in the earlier works. These

improvements in calculating kerma only became apparent at energies greater than 10 MeV. Below 10 MeV the values showed generally good agreement with the earlier work (Bach and Caswell, 1968). The most recent compilation of kerma extended the energy considered to 30 MeV (Caswell et al., 1976) (ICRU, 1977). Table 2 shows the various values of kerma at 14 MeV for standard man tissue.

Table 2. Kerma at 14 MeV

Kerma $(erg/g)/(n/cm^2)$	Source
6.67×10^{-7}	(Ritts et al., 1971)
6.42×10^{-7}	(Bach and Caswell, 1968)
7.10×10^{-7}	(Auxier et al., 1968)
6.40×10^{-7}	(Caswell et al., 1976)

At 14 MeV, values shown in the table differ in the worst case by about 11%. Agreement at lower energies is much better, and overall, discrepancies in kerma found in the literature are not excessive considering the slight differences in tissue composition, different assumptions used to generate kerma, and uncertainties in the cross sections themselves.

The work of Auxier et al. (1968) is noteworthy in that it gives calculations of LET using a method first developed by Snyder (1964). While this work did not present a table of LET as a function of neutron energy, it did present changes that occur in LET because of spectral changes that occur with changes in depth. Using a 60 cm high cylinder, 30 cm in diameter, these workers also produced depth dose calculations from a Monte

Carlo code. The work was later incorporated into NCRP Report 38 (NCRP, 1971). With broad-beam irradiation, depth dose differed from the earlier calculations in a semi-infinite slab primarily in that neutron capture gamma dose was greater in the slab. Since this code possessed the capability for calculating LET, it was used as a basis for the code developed for this dissertation.

Recognizing the complexity of the total problem, others have calculated the charged particle spectra released by fast neutrons in tissue (Caswell and Coyne, 1972). This work presented not only the initial spectrum of charged particles, but also an "equilibrium" spectrum which occurs when the charged particles are stopping. Unfortunately, these data were calculated for only two neutron energies, 1 and 14 MeV. Moreover, the data were not suitable for incorporation into a Monte Carlo code to calculate LET. That work has been extended to more energies but is not complete enough to permit incorporation into a Monte Carlo calculation (Caswell and Coyne, 1973).

Depth dose calculations using Monte Carlo techniques have undergone considerable development. Jones and co-workers altered the cylinder previously described to permit study of the effect of finite beam size (Jones, Snyder, and Auxier, 1971). In that work, a 5 cm diameter parallel beam of neutrons impinged unilaterally on the 30 cm diameter cylinder of tissue. Dose from ions and photons produced by neutron beams of several energies was studied over the region in and near the neutron beam, and results were compared with broad-beam calculations. The depth dose curves from recoil ions and gammas produced by neutron interactions showed less

penetration than the broad-beam results. At 14 MeV neutron beam energy, the high LET fraction of the dose delivered by recoil ions decreased with depth in the beam, near the beam and far from the beam. More applicable to the present work, the LET spectra showed only slight change with depth from 14 MeV neutrons. One conclusion that can be drawn from this work is that with either increasing depth, or increasing distance from the beam axis, the low LET component becomes more significant.

Wilkie simulated a human torso by extending a cross section of the chest in the third dimension to form an elliptic cylinder (Wilkie, 1970). Using a Monte Carlo code, Wilkie calculated dose distributions from recoil nuclei for both broad and collimated beams of 14 MeV neutrons. Depth dose curves in his work showed a dramatic change from a homogeneous elliptical cylinder to a heterogeneous one with lung and bone.

Related Experimental Work

With the vast amount of published material in neutron dosimetry, a complete review would be impractical. Because of this, the discussion will be limited to those recent measurements which verified calculational models and those with applicability to 14 MeV neutron radiotherapy.

An experimental comparison with the man-sized cylinder phantom calculations by Auxier et al. was made in 1971 (Chen et al., 1971). Measurements were done using a Hurst phantom proportional counter for the fast neutron dose and a "Phil" (shielded G-M tube) for gamma dose. At 14 MeV incident neutron energy, agreement of experimental data with the theoretical results is well within the standard deviation.

Two other investigations of fast neutron depth dose distributions were dissertations at the Georgia Institute of Technology (McGinley, 1971; Poston, 1971). Poston measured depth dose distributions near bone tissue interfaces using an extrapolation ionization chamber technique suggested by Failla (1937). Total dose was measured near the interface, with no attempt to separate the total into gamma and heavy ion components. McGinley utilized a paired system of a TE ion chamber and thermoluminescent detectors to separate the dose components. He studied the results at greater distances from bone, and showed general agreement with Poston's work.

McGinley also developed depth dose data for an ellipsoidal phantom with a cross section similar to the Reference Man phantom torso region without the skeleton. This work was compared with Wilkie's calculations and some differences were observed. The discrepancy was explained by McGinley as being due to a difference in beam size (Wilkie assumed a broad beam, McGinley used a beam 18.4 cm square), and the fact that Wilkie's data have no inverse square loss whereas McGinley's experiment used a nearly point source. McGinley has recently extended this work to another neutron spectrum currently in use for fast neutron therapy (McGinley and McLaren, 1975). This neutron source is a cyclotron which is used to produce neutrons of approximately 15 MeV average energy by bombarding beryllium with 35 MeV deuterons (Theus et al., 1974). This beam shows similar penetration to monoenergetic 14 MeV neutrons from the D-T reaction (Bewley, 1971). Somewhat greater shadowing behind bone was observed with these spectra (McGinley and McLaren, 1975).

In work comparing their own measurements of collimated beams of

neutrons with others, Broers-Challis and her co-workers exhibited graphs showing little improvement in penetration from collimated D-T neutrons at 125 cm SSD (source to skin distance) (data from Goodman et al., 1970) to an infinite SSD as calculated by Jones (Jones et al., 1971)(Broers-Challis et al., 1974). Agreement was also shown between their measurements at 45 cm SSD and earlier work by Green and Thomas at 50 cm (Green and Thomas, 1968).

The study of Broers-Challis was preceded by measurements made for the Rijswijk preclinical fast neutron therapy trial (Broers et al., 1972). The measurements included depth dose measurements across the chest using a collimator which is similar to the one employed for this dissertation. Results were reported for a Rando-type phantom with a foam rubber lung.

The work at Rijswijk was later extended to study depth dose distributions at several SSD's up to 100 cm. In that work, lungs similar to those used by McGinley were placed in a 30 cm cube of water (Mijnheer et al., 1974). Their depth dose tables showed somewhat less penetration than those of Green (Green et al., 1968). This was attributed to the use of polyethylene in the collimator resulting in more low energy neutrons in their spectra.

Beach and Kelsey evaluated collimator scatter and patient scatter at 125 cm SSD for D-T neutrons (Beach and Kelsey, 1975). Collimator throat scatter* was found to affect depth dose. Depth dose showed increased penetration with larger field sizes.

Dosimetry intercomparisons are important because they allow pooling

---

*Throat scatter refers to small angle neutron scattering in the part of the collimator opening nearest the target.

of patient populations permitting faster evaluation of various protocols. Evaluations of dosimetry practices in the United States (Smith et al., 1974), in Great Britain (NPL, 1974), and in Germany (Maier et al., 1974) allowed this dissertation work to draw on expertise and common practice at the various neutron therapy centers. Recent recommendations by the ICRU also proved helpful in providing values for various parameters required to evaluate data (ICRU, 1977). Agreement in the literature between calculated and measured LET spectra is not as universal as is the case with depth dose. LET spectra do not exhibit major change with depth for 14 MeV neutrons. In one set of measurements, Paretzke observed a regular decrease in the high LET portion and an increase in the low LET portion of the spectra as the depth increased. This was attributed to a gradual softening in the neutron energy spectra (Paretzke et al., 1972). Calculations shown in that same paper did not agree with measurements in the LET spectra above 40 keV/μ. This was attributed by the authors to the oxygen (n,alpha) reactions in tissue which are less probable in tissue equivalent plastic because of the substitution of carbon for the oxygen. Other LET calculations showing changes with depth do not show a regular decrease in the high LET component with increasing depth (Jones et al., 1971).

Summary of Previous Work

Calculations of kerma received considerable attention over the past decade and are advanced to the point where further development is difficult to achieve. Likewise, calculations of dose to man-sized masses of soft tissue exist for a large variety of irradiation conditions. However, relatively few calculations exist for more realistic, anthropomorphic geometries.

Similarly, while many measurements are reported for homogeneous phantoms and while a number of authors have studied the effects of lung, no measurements have attempted to simulate skeletal structures. Experimental studies with bone have examined effects at the bone-tissue interface, or from large bone cylinders.

Few measurements exist which compare with calculations in an absolute manner. In general, results are either normalized to the peak value of dose beneath the phantom surface, or are given relative to some monitor.

As was stated in the objectives in Chapter I, this research will develop the necessary codes to calculate dose and other parameters in an anthropomorphic phantom. In addition, it will develop dosimetry techniques to verify the calculations and will attempt to compare the calculations and measurements against one another in an absolute manner.

CHAPTER III

REVIEW OF CODE DEVELOPMENT

No Monte Carlo code was available with all of the features needed to fulfill the objectives of this dissertation. A study was undertaken to examine the capabilities of several code packages available from the various code distribution centers. The results of this study showed that, while recent codes were desirable because of programming support supplied by the code distribution centers, none of the codes possessed the capability to calculate LET. Therefore, an older code which had this capability was utilized as the basis for the neutron transport calculations. This chapter describes the tradeoffs made in selecting this code and documents the input data used and coding decisions made for the calculations. Results are presented in a later chapter.

Features of the Monte Carlo Code Developed for This Dissertation

The code to transport neutrons through the Reference Man was developed from one used extensively for health physics calculations (Auxier, Snyder, Jones, 1968) (Jones, Snyder, Auxier, 1971). This code was originally derived from the 05R neutron transport code and the OGRE photon transport code. Neutron cross sections for the four most important elements in man (hydrogen, carbon, oxygen, and nitrogen) were those used previously with this code. Cross sections for other elements were ob-

tained from ENDFB/IV using the AMPX system. Photon cross sections were generated from ENDFB/IV from programs in the OGRE system. Plots of the mean free path for neutrons and photons as a function of particle energy are shown in Figures 5 and 6, respectively, for the three regions of Reference Man. As was observed with the kerma plots in a previous section, the curves for all three regions parallel each other for either photons or neutrons. The differences in the curves reflect density changes and changes in hydrogen content.

In this code, neutron cross sections were stored as point energy cross sections. To represent adequately such a cross section, a large number of points was required. This causes the large resonances in the cross sections to be reflected in the neutron mean free path at high energy. With the averaging which is inherent in the Monte Carlo process, these resonances are not significant.

The geometry used for Reference Man was taken from ALGAM. Figure 7 is taken from that work, and shows the internal organ structure of the phantom. The stopping power code SPAR, which incorporates all of the features discussed earlier, was used to generate stopping powers for all of the charged particles in all three regions of Reference Man. These are shown in Figures 8, 9, and 10 for total body, lung, and skeletal tissue. To show the difference in stopping for the same particle in the three regions, Figures 11 and 12 show stopping for protons and oxygen ions, respectively in the three regions. The technique used in the code for obtaining dose as a function of LET was that developed by Snyder (1964).

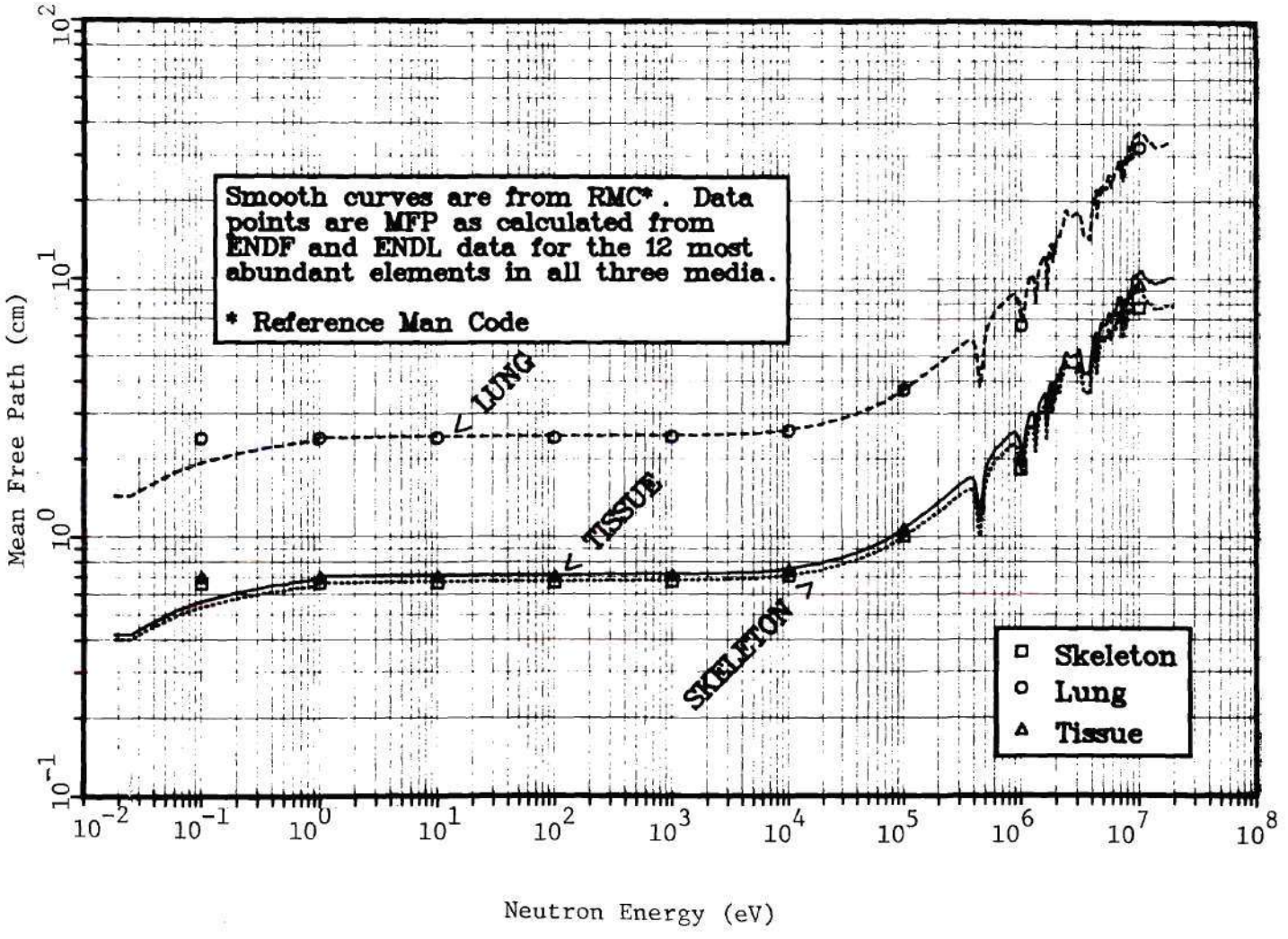

Figure 5. Mean Free Path of Neutrons in Reference Man

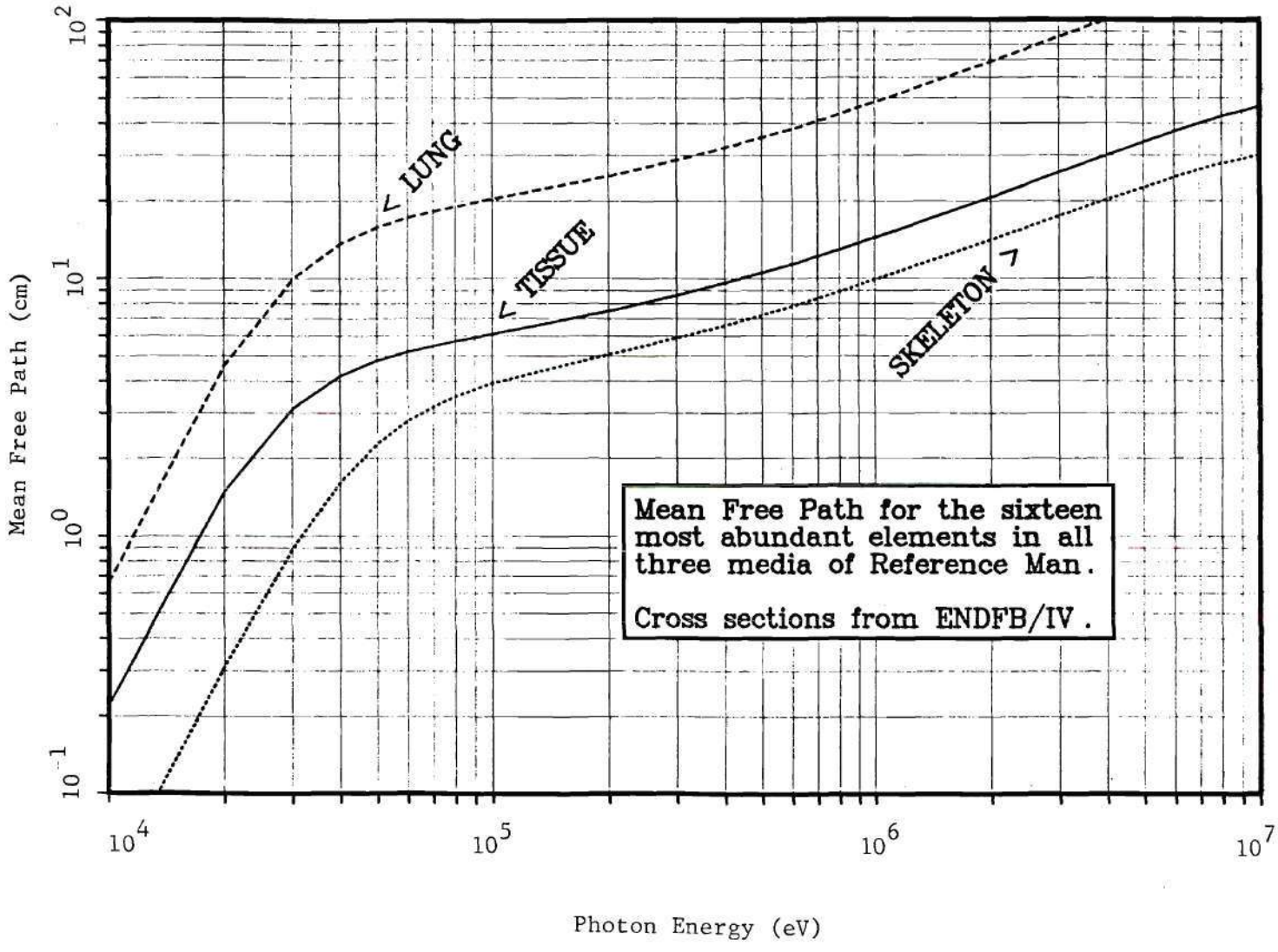

Figure 6. Mean Free Path of Photons in Reference Man

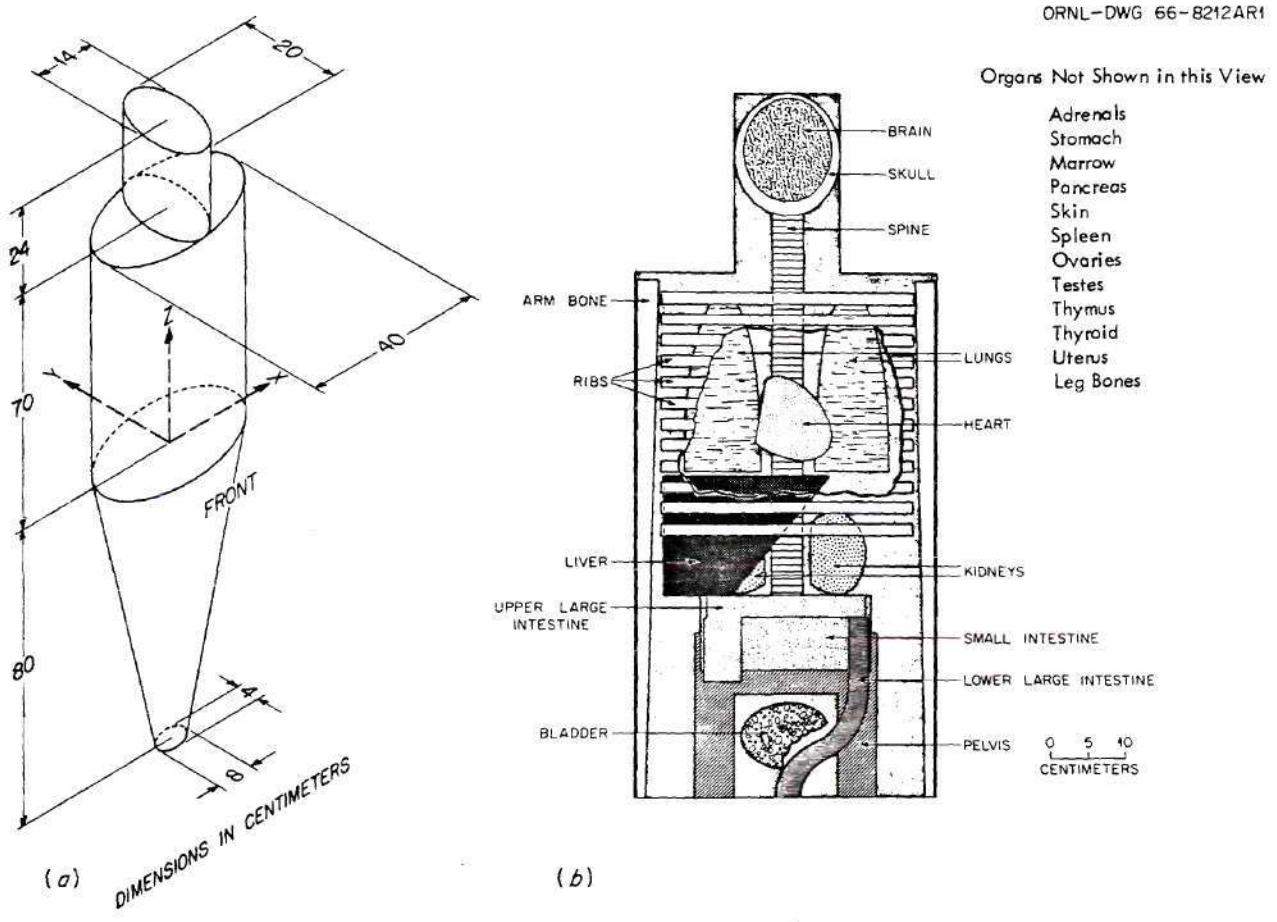

Figure 7. The Adult Human Phantom Showing Organ Structure and Coordinate System

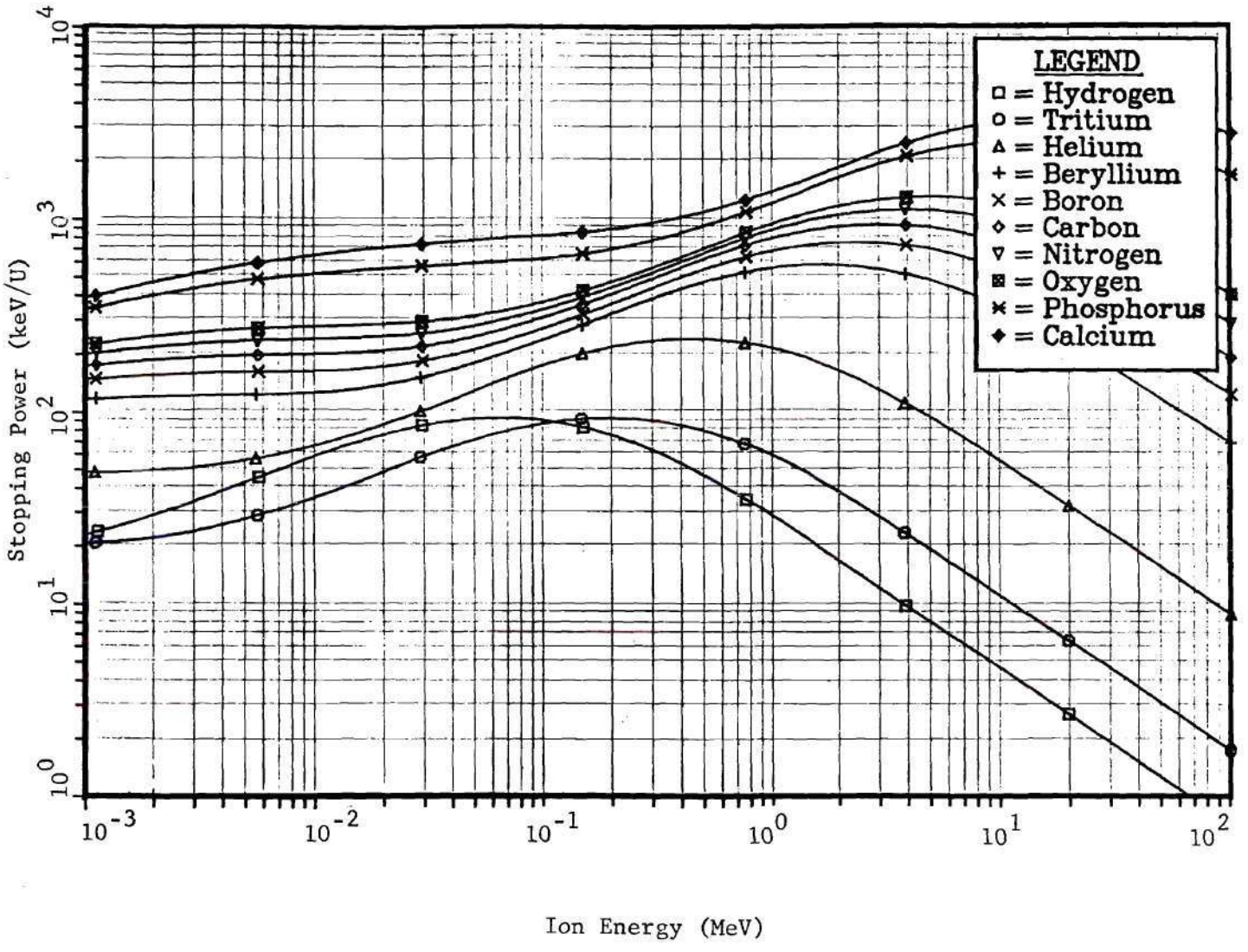

Figure 8. Stopping Power of Ions in Reference Man Soft Tissue

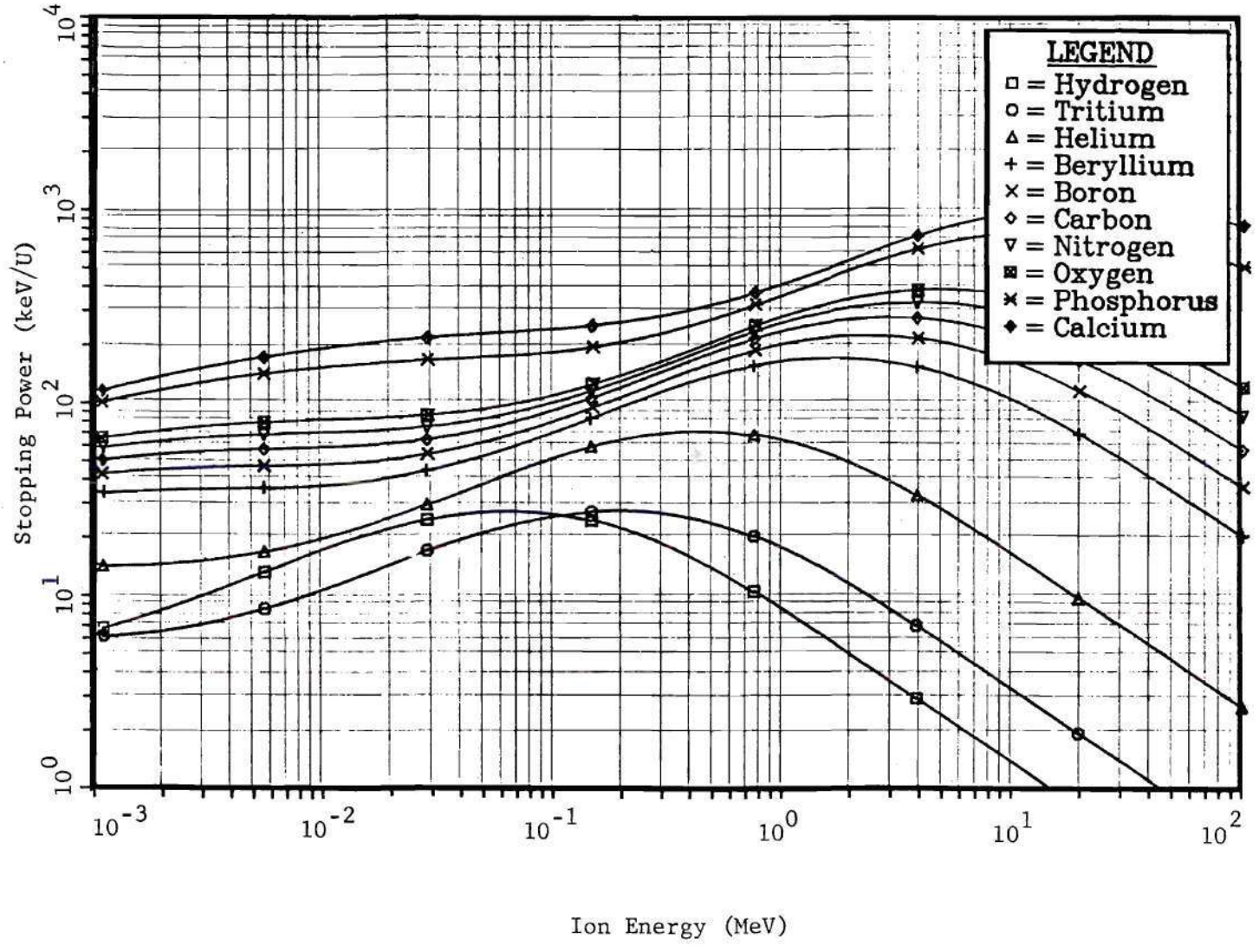

Figure 9. Stopping Power of Ions in Reference Man Lung

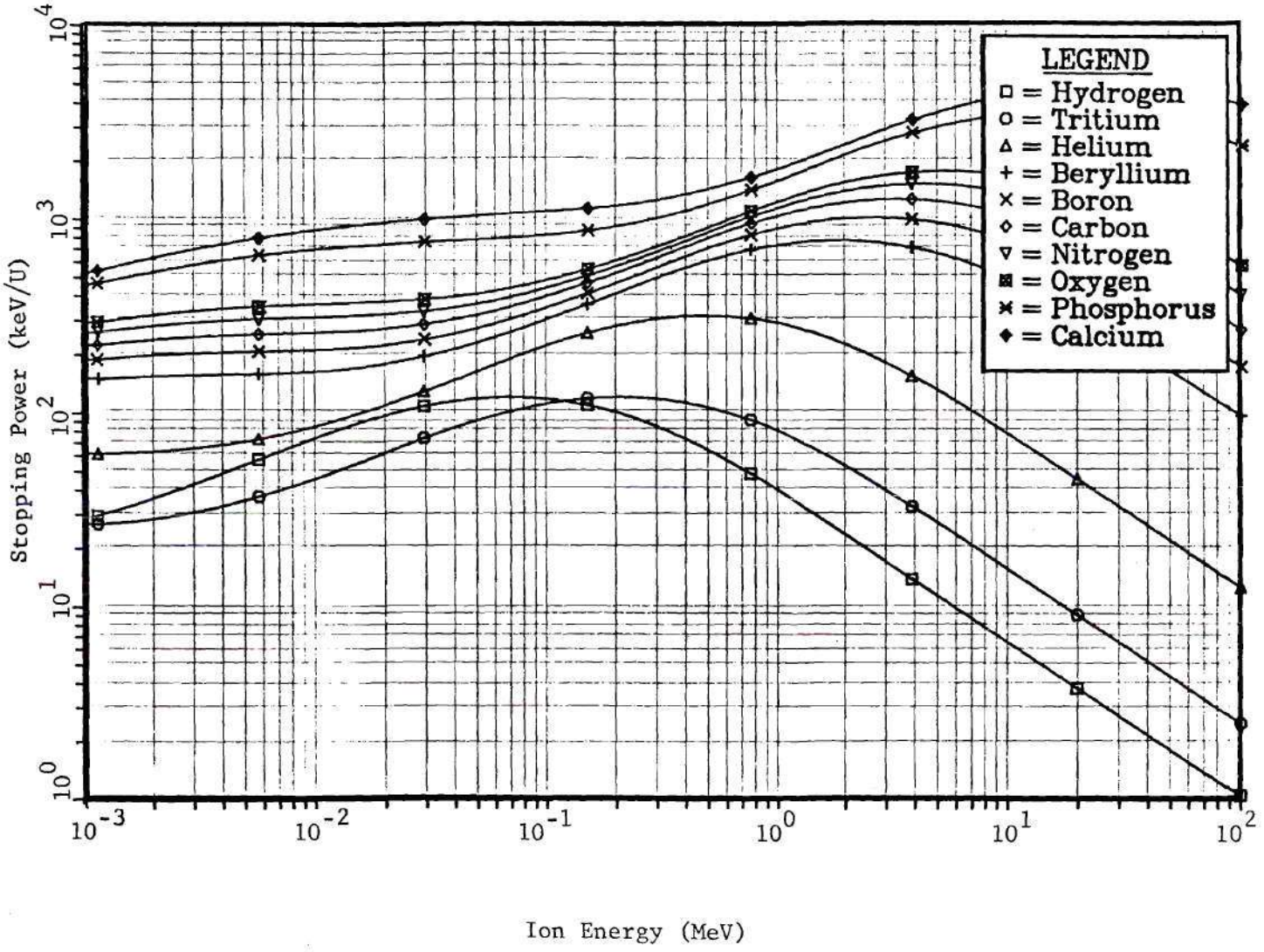

Figure 10. Stopping Power of Ions in Reference Man Skeleton

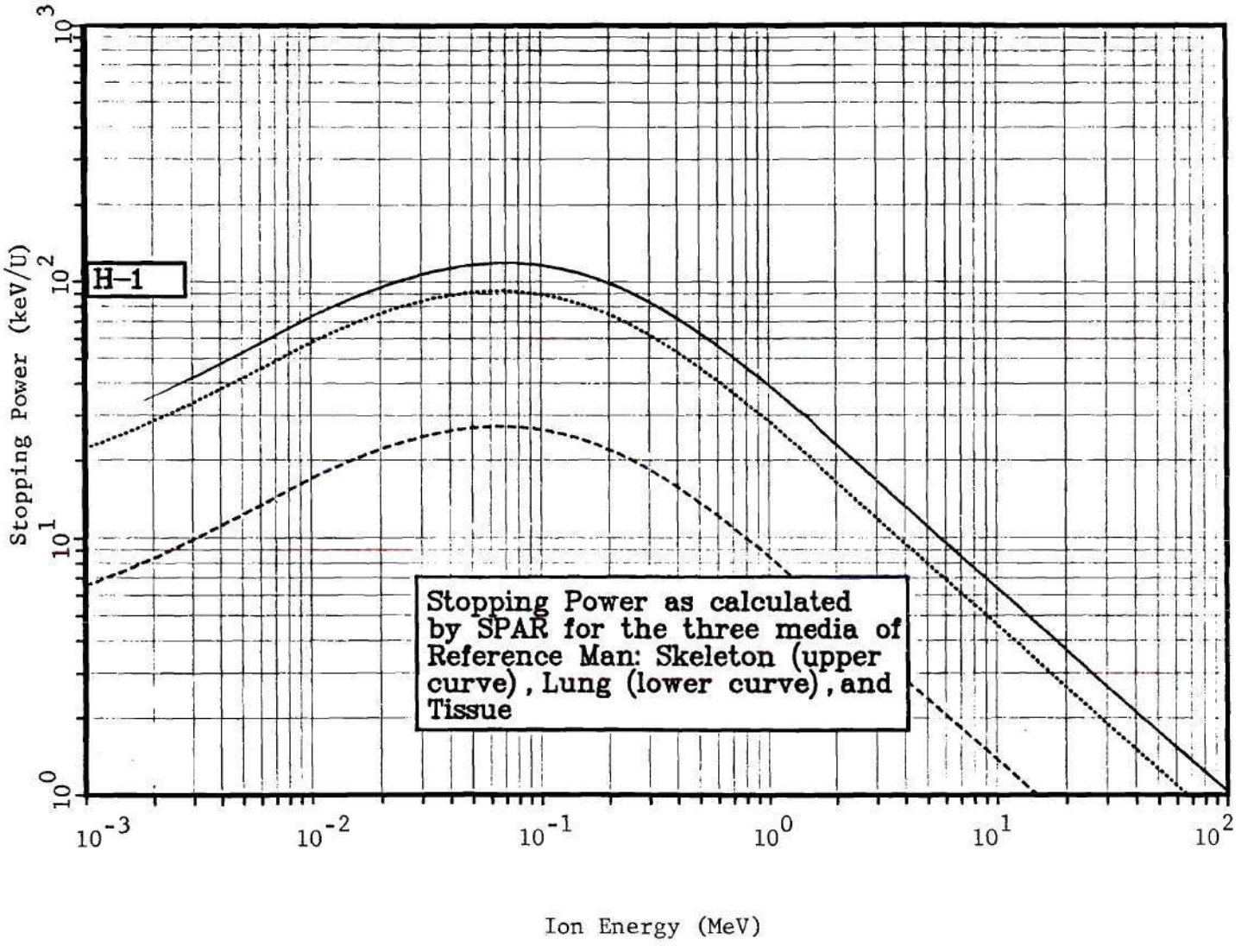

Figure 11. Stopping Power of Hydrogen Ions in Reference Man

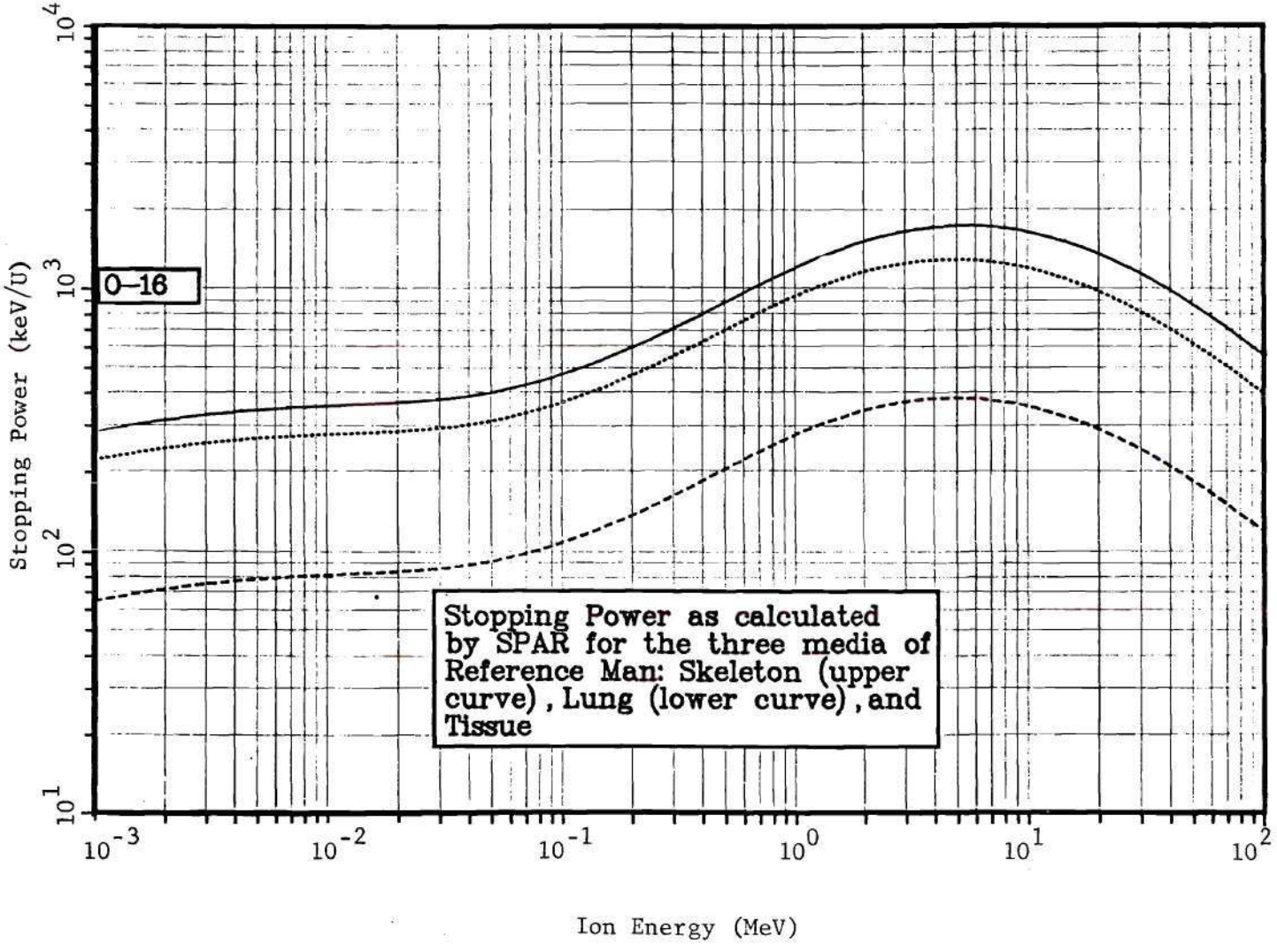

Figure 12. Stopping Power of Oxygen Ions in Reference Man

Available output from the code included neutron absorbed dose, dose equivalent, LET distributions, and neutron spectra at up to 25 sites. The LET distributions at sites in lung or bone were computed as if the media were tissue. This was done in an attempt to match experimental measurements more closely. In addition to this, average dose was tabulated in each of the organs. The photon dose was output in both the sites and organs. The location and size of the sites were chosen to correspond to points at which experimental data were taken.

The source routine was developed from well-known energy-angle relationships for the D-T reaction. Neutrons started on the target were given an appropriate energy for their direction of travel. The collimator was an ideal aperture in that only those neutrons transiting the hole in the collimator were transported through the phantom. The dose was normalized to the total neutron output (4π) from the target.

Features of Related Codes

The code developed for this dissertation was derived from the 05R code (Irving et al., 1963). Code 05R has been the progenitor of at least two other codes, ESP and MORSE (Straker et al., 1970). All three of these codes treat the physics of the scattering process in the same manner. ESP and MORSE were the result of development in 05R over a 10 year period, with MORSE being the latest version. As such, differences between these three transport codes reflect the increasing sophistication of the Monte Carlo technique. There are two areas where this development has

resulted in real differences in the codes: the treatment of cross sections and geometry. The code described in the previous section differs from these three codes in another major respect, i.e., the manner in which dose and LET are calculated. The differences in cross section treatment, geometry, and dose calculation among these codes are described below.

The significant change in cross sections has been the development of multigroup cross sections. Code 05R and the code developed for this dissertation treat cross sections as the value at a given energy. MORSE treats cross sections as the value for a neutron group which might encompass a wide range of energies. In general, this multigroup approach requires less detail in the cross section library. The primary advantage of this technique is derived from the fact that photons are treated in exactly the same manner as neutrons. A probability for a decrease in energy is treated the same as a probability for gamma production. With a properly prepared cross section library the entire problem can be treated at once. With older codes, the photons produced by neutron interactions were stored for transport by a separate code. In addition to reducing a transport problem to a single step rather than two separate ones, the multigroup technique permits the solution of the adjoint problem. This adjoint technique solves the Boltzmann transport equation backwards. The approach starts with an educated guess of the final spectra and transports the particles backwards to the source, increasing energy at a scattering event. The actual source is compared with the one obtained from the adjoint problem and a new guess is made. Iteration gradually alters the final spectra until the source calculated matches the actual one. Significant computer

time savings can be obtained in deep penetration problems by solving the adjoint problem in this manner.

The second area where there has been development is in the geometry. One of the major tasks in setting up a Monte Carlo problem is coding the system geometry. The 05R generalized geometry required the user to create a quadratic equation for each surface. Combinatorial geometry, a recent development used by MORSE, permits a user to create a region by combining various geometric figures already stored. The code developed for this work utilizes a simplification made possible by use of the hole routine which is a technique for transporting particles across boundaries (Warner et al., 1968). The method considers an internal region as a hole in the basic region. In a series of collisions, the hole routine tracks a particle by computing the next collision site based on the smallest mean free path. The mean free path of the medium at a collision site is compared with the one used for selecting that site. If the mean free path is different, a game of chance is played in which the chosen site is compared to one selected using the actual mean free path. If the site is rejected, the particle continues along its path. In general, the hole routine is chosen if there are more collisions than there are boundary crossings. The use of the hole routine in this work did not utilize this criterion but instead served to simplify the geometry. The entire phantom was surrounded by a parallelepiped. This parallelepiped formed the system geometry. All body organs were considered to be holes.

The final difference among these codes is in the calculation of dose and LET. Codes 05R, ESP, and MORSE all use kerma factors computed prior to

the transport problem to compute dose. At a collision site in a region of interest the energy of the neutron was used to look up kerma in a table. In this work, the neutron energy was used to look up a reaction in a probability table and the energy of the reaction products was used to compute kerma and LET. While this approach is inefficient, it permits the calculation of LET. LET as a function of neutron energy for the three media in Reference Man is an important parameter which has not been available in the literature.

CHAPTER IV

EXPERIMENTAL PROCEDURE

Objective

To test results of the Monte Carlo code three pieces of information were required from the experiment: photon dose, neutron dose, and dose as a function of LET. There is a wide variety of detectors capable of measuring these parameters. Table 3 is adapted from Goodman (Goodman, 1974) and shows in general terms the relative sensitivity, energy dependence, and accuracy estimated by him for several detectors. Choice among these detector systems depends not only on availability and suitability but also on personal expertise, since the accuracy quoted is the best obtainable. An optimal system in terms of accuracy and ease of use is obtained with the ionization chamber and Geiger-Müller counter. A gas flow tissue-equivalent ionization chamber with a nominal one half centimeter volume is available commercially. Its size makes it well suited for in phantom dosimetry, and being tissue equivalent, the chamber conforms reasonably to the Bragg-Gray principle and does not significantly alter the radiation field. Because of the importance of accurate neutron dosimetry the material used in its construction (A-150 plastic) has been the subject of a recent study (ICRU, 1977). This study recommended a value for kerma factor as a function of energy for the plastic and its recommendation is used by all neutron therapy centers with A-150 plastic chambers. Likewise the energy-compensated G-M tube has been the subject of a recent study to determine

Table 3. Characteristics of Fast Neutron Dosimetry Systems (from Goodman, 1973)

Dosimeter	Accuracy (%)		Relative Sensitivity (%)		Neutron Energy Dependence Relative to Tissue
	Neutron	Photon	Neutron	Photon	
TE Ion Chamber	5-10 (p)	2-5 (p)	100	100	very low
TE Proportional Counter	5-10 (m)	--	high	high	very low
Thermoluminescent Material	10-20 (p)	10-20 (p)	3-35	moderate	moderate
Energy Compensated Geiger-Müller Counter	--	6 (p)	0.1-3	high	--
Non-hydrogeneous Ion Chamber	--	3-20 (m)	2-30	~ 100	moderate

NOTE: (p) = pure field; (m) = mixed neutron and photon field

its fast neutron energy dependence (Lewis and Young, 1977). The application of a sophisticated coincidence technique permitted a highly accurate measurement of the fast neutron response.

Measurement of dose as a function of LET can be accomplished in several ways as well. One commercially available technique utilizes a proportional counter of the Benjamin design (Benjamin et al., 1968). This detector has walls constructed of tissue-equivalent A-150 plastic. This device is in use at most neutron therapy centers in the United States and is the most widely used device for measuring LET. The small size permits its use in a phantom.

A decision was made to simulate the experiments performed for the Rijswijk preclinical trials. This was done for two principal reasons. First, the Rijswijk preclinical trials formed the basis of an ongoing clinical program in Amsterdam and also were designed to obtain fundamental radiobiological data. Any additional information on physical parameters might enhance this work. Secondly, the Snyder-Fisher mathematical model seemed particularly well suited to simulate the irradiation conditions in the thoracic region. Their work could provide a direct comparison for some of the data generated for this dissertation.

To simulate the Rijswijk geometry, a collimator similar to the one used by the Dutch was built. An accelerator facility was modified to provide irradiation conditions nearly identical to those at Rijswijk, and a plastic analogue of the mathematical model was constructed. Some of the phantom pieces were available from other experimental work at the Oak Ridge National Laboratories (Garry, et al., 1975).

The phantom, which comprised the trunk section of the mathematical model, was placed in the beam of neutrons. The neutron and photon doses were measured as a function of depth for four conditions: the phantom filled with TE fluid only, with lung and TE fluid, with skeleton and TE fluid, and with lung, skeleton and TE fluid. These four conditions allowed the data to be analyzed to separate the effects of lung and bone. An additional experiment measured the LET spectra at the front, middle and back of the phantom with lung, bone, and TE fluid.

The remaining sections in this chapter describe the equipment used for simulating the Rijswijk configuration. Also described are techniques used for analyzing data and the methods used for error analysis.

The Accelerator

The accelerator used for this experiment as a neutron source was the "Dosar" Low Energy Accelerator (DLEA) which is a modified Texas Nuclear model 9999. Modifications included the addition of a sulfur hexafluoride tank and new transformer to permit operation at 200 kV with 1 mA of beam current. The accelerator was located in a 6m x 10m room and was positioned along a diagonal of the room with the target in the center. This is shown in Figure 13. The machine was further modified for this work by the addition of a PdAg leak for the ion source, the use of an ORTEC type RF ion source, and the addition of a silicon surface barrier diode for measuring neutron output by the associated particle technique. The diode was located off the beam axis in the drift tube. A long counter with a Nancy Wood BF_3 tube was used as a secondary means of normalization and was located in a fixed position six meters from the target. The cooling system for the

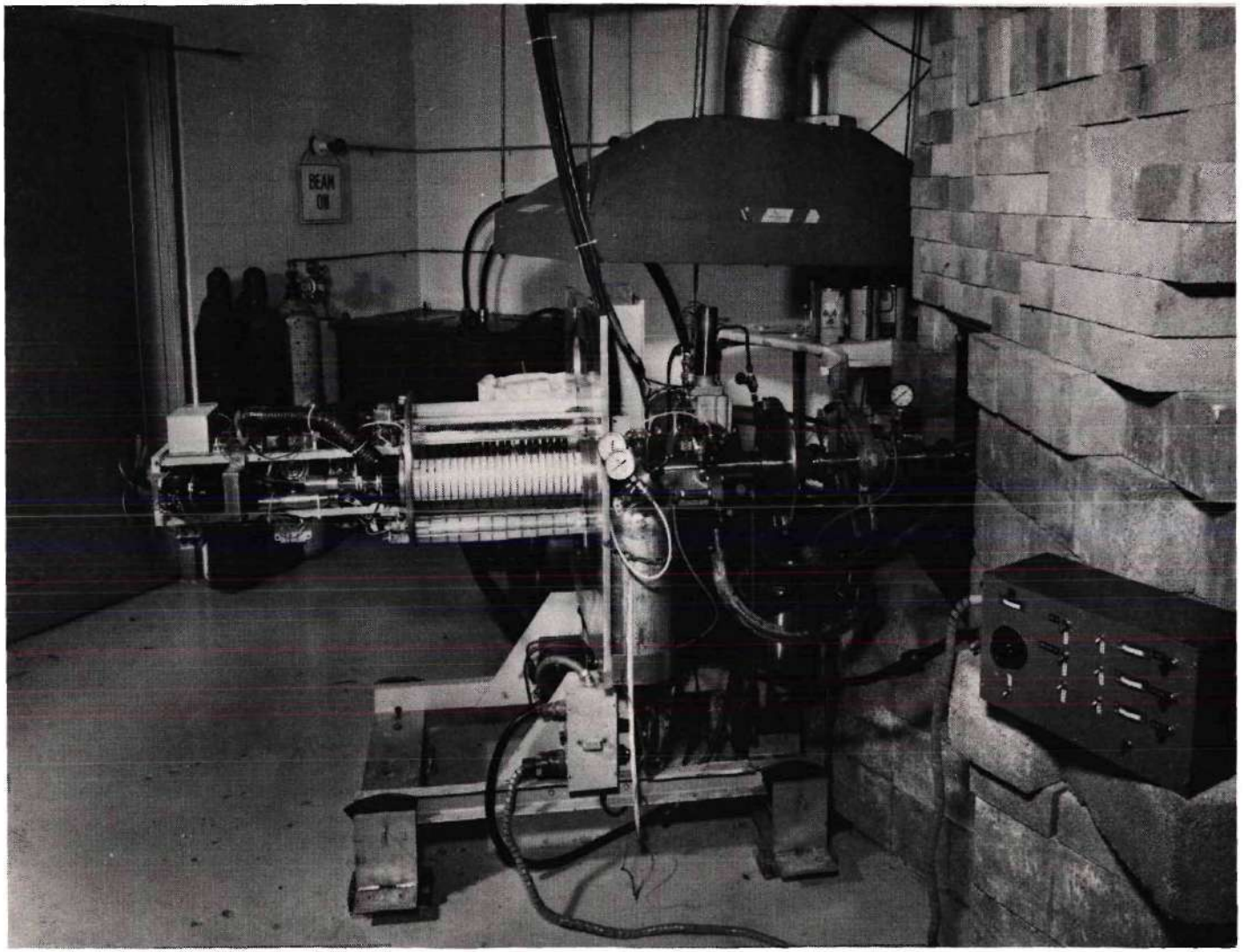

Figure 13. Photograph Showing Accelerator and Shielding Wall

target was improved by using larger tubing (3/8 inch) for supply and return lines and by using a water-ethylene glycol solution instead of water, which permitted cooling below $0^{o}C$ by a refrigeration unit. Figure 13 shows a photograph of the accelerator with the collimator and shielding wall in place.

The targets were thin copper foils 32 mm in diameter with an active area 25.4 mm in diameter containing titanium-hydride loaded with 16 Ci of tritium. An associated particle detector was located 44 cm from the target and was 6.4 mm in diameter. As count rates would have exceeded the capabilities of the electronics, the alpha detector was fitted with a brass collimator cap with a 1 mm hole. This resulted in 3.1×10^{-7} alpha particles counted for every neutron emitted from the target.

Collimator and Shielding Wall

The collimator was constructed to conform to the dimensions used in the Rijswijk preclinical studies. This collimator is depicted in the insert in Figure 14. The thickness of the collimator was 41 cm overall, comprised of alternating layers of steel and polyethylene (PE), 70 x 70 cm in size. Starting from the target end, the laminations were successively 5 cm PE, 15 cm steel, 5 cm PE, 5 cm steel, 5 cm PE, 5 cm steel finally covered with a 1 cm sheet of lucite. A 10 x 10 cm hole was cut from the center of each sheet and a steel insert was machined to fit this hole tightly. The insert had a cavity which defined a 6 x 8 cm hole on the surface of the phantom, and tapered to a 3 x 3 cm hole at the target end. The accelerator was positioned to a 45 cm SSD. A 3 mm sheet of Teflon used at Rijswijk over the collimator opening to restore skin sparing was

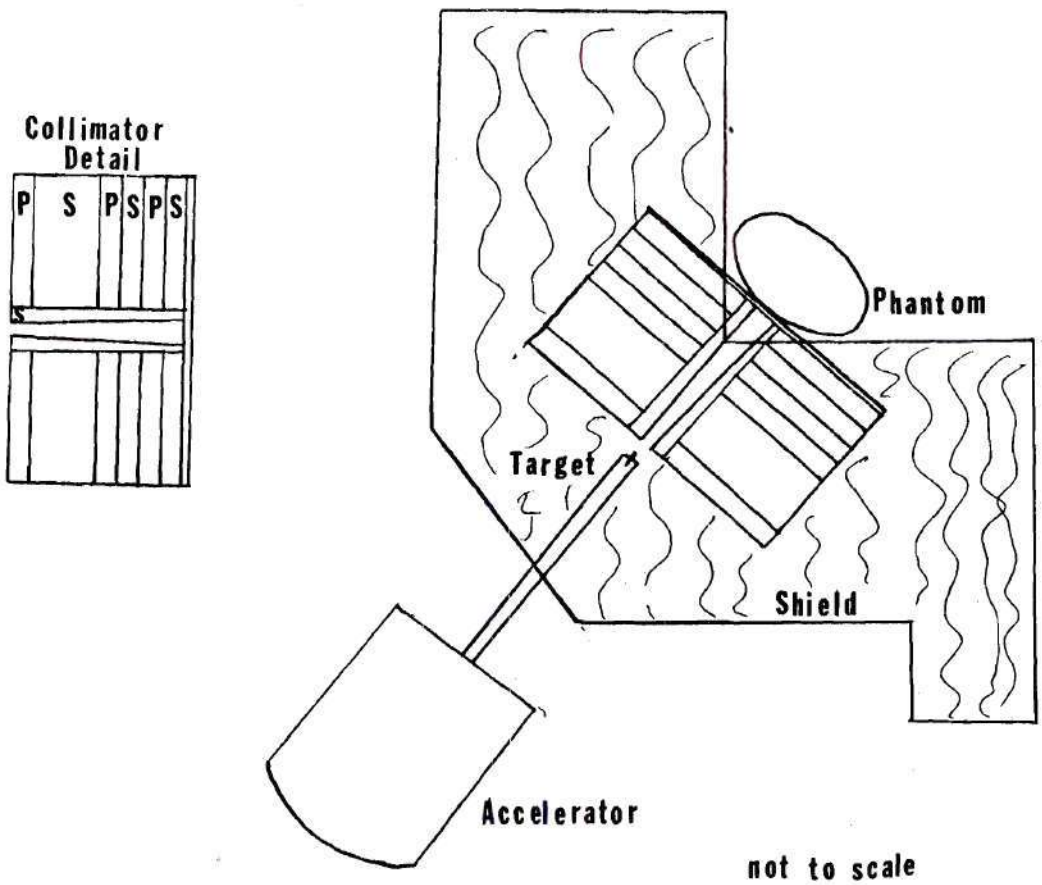

Figure 14. Drawing of Accelerator, Shielding Wall and Collimator Configuration. Insert Shows Collimator Detail.

not employed for this research. A fast neutron beam exhibits skin sparing in air. The final lucite sheet in this collimator released protons which eliminated any skin sparing. Teflon contains no hydrogen and restores skin sparing.

The collimator was positioned in the corner of an L shaped concrete block wall which provided a minimum of one meter of concrete shielding to the experimental area. The configuration of the shield, collimator and accelerator is depicted in Figure 14. The input of the electrometer exhibited radiation sensitivity and indicated current flow when exposed to gammas with or without an ion chamber attached. A lead cave 15 to 20 cm thick was built into the wall in a position as far from the target as possible. This cave was used to shield the remote reading electrometer. The dose rate in the experimental area outside the beam was greatest near the phantom, apparently due to capture gammas produced in the phantom.

A laser backlighting technique was employed as an aid to alignment for the experiments. In this method, a small laser beam is directed to intercept cross hairs positioned at the front and rear of the collimator aperture. The accelerator was positioned on the axis defined by the laser beam at 45 cm SSD. The phantom was then positioned using fiducial lines etched on the front and rear surfaces of the phantom corresponding to the midplane of the left lung.

Normalization of Data

Most depth dose and LET work in neutron dosimetry utilizes a relative normalization. That is to say, every measured point is divided by the largest value and plotted in terms of percent. One of the unique

features of this research is an absolute normalization. Two channels of neutron output were measured for each experimental point. These allowed data points to be given in terms of dose per neutron emitted from the target and permitted an absolute comparison with the calculational results from the Monte Carlo code. The two normalization signals were obtained from an alpha particle detector used to detect the alpha emitted in the D-T reaction and a precision long counter for neutron detection.

This associated alpha-particle technique for determining neutron yield from the D-T reaction turned out to be an elegant arrangement in that few corrections were required to measure yield. In practical terms, a knowledge of the distance of the alpha detector from the target, the diameter of the detector, and the angle between the beam axis and the detector-target axis are all that are needed to compute the constant to convert alpha counts to neutrons emitted.

In the system utilized for this experiment a small silicon surface barrier detector (6.4 mm in diameter) was placed in the drift tube 44 cm from the target. A brass collimator cemented in place limited the diameter seen by the alpha particles to 1 mm. A preamplifier, amplifier, and single channel analyzer (SCA) were used at the accelerator. Pulses from the SCA were sent via a long coaxial cable to a scaler located in the control room. Twelve volts of bias voltage was required to optimize the signal to noise ratio. A ^{241}Am alpha source and a pulser were used to calibrate the system initially. A multichannel analyzer located at the accelerator facility and operated from the control room was used to verify the SCA set-

tings during some of the initial runs. The overall correction factor to convert scaler counts to neutrons emitted was 3.26×10^6.

A long counter arrangement with a Nancy Wood BF_3 tube was mounted approximately 6 m from the target and provided a second check of neutron output. This tube differs from a standard BF_3 tube in that boron depleted in ^{10}B is used, resulting in a decrease of neutron sensitivity. A conventional tube located anywhere in direct sight of the target would have experienced count rates exceeding the capabilities of the available counting circuits. The counts from the long counter varied linearly with neutron output, and thus it was possible to calibrate the long counter against the associated particle detector as a second means of normalization. This proved to be fortunate since the surface barrier detector failed midway through the experiment. A factor of $1.97 \pm 1.7\%$ was calculated from the initial runs making each long counter count correspond to 6.42×10^6 neutrons with small uncertainty. Because of its availability for all experiments, all normalization procedures made use of the long counter.

The Phantom

An experimental phantom was needed that closely matches the mathematical model and permits access for dosimeters. The phantom was constructed from thin plastic shells which detailed bone structure, lungs, and exterior surfaces. These shells were then filled with bone-, lung-, and tissue-equivalent substances. The plastic of the shells was considered part of the soft tissue region. Figures 15, 16, and 17 show the complete phantom, the left lung with its access holes for dosimeters with tubes to

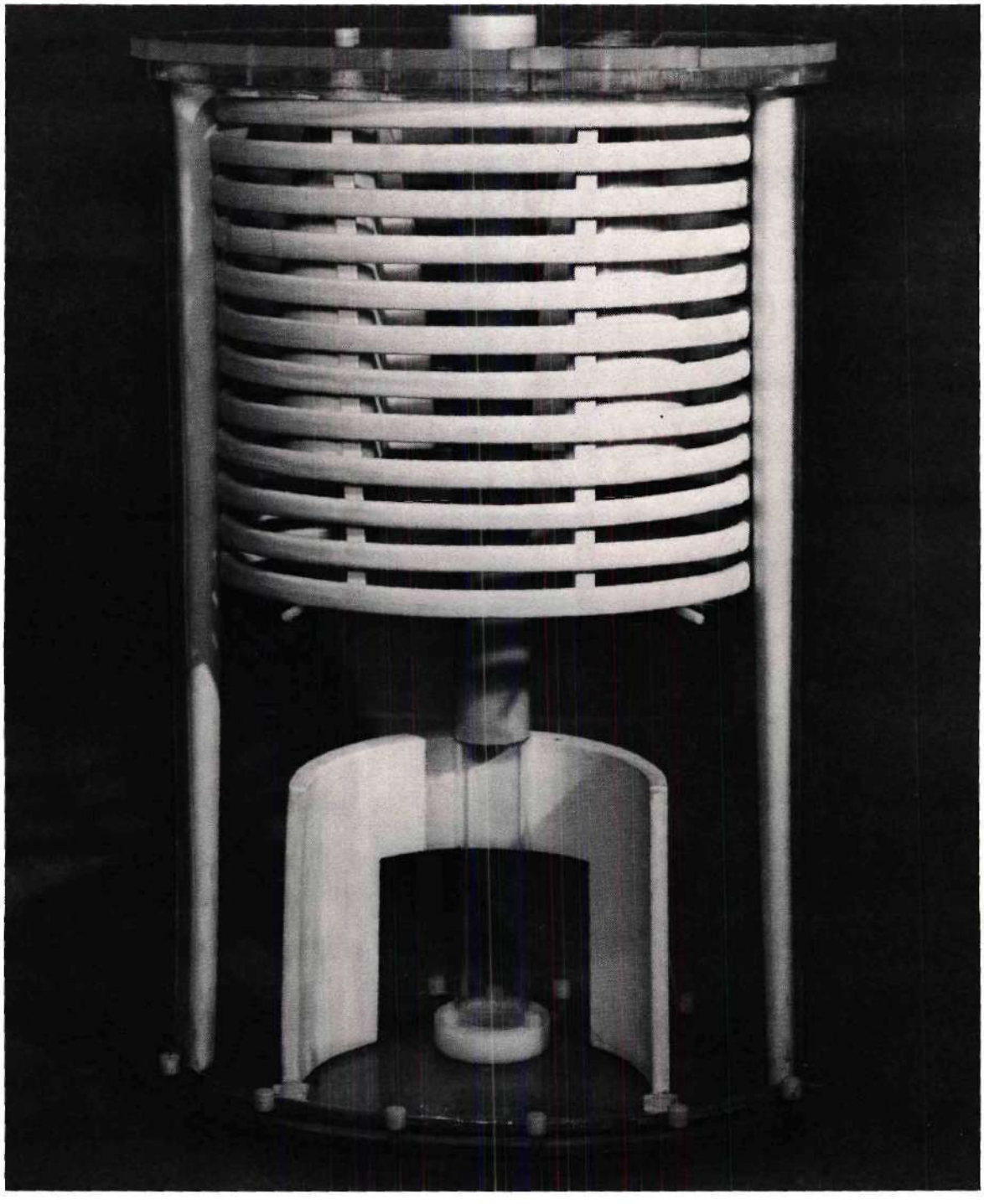

Figure 15. Photograph Showing Complete Phantom Without Tissue-Equivalent Fluid. Phantom Is a 70 cm Tall, 20 x 40 cm Ellipse.

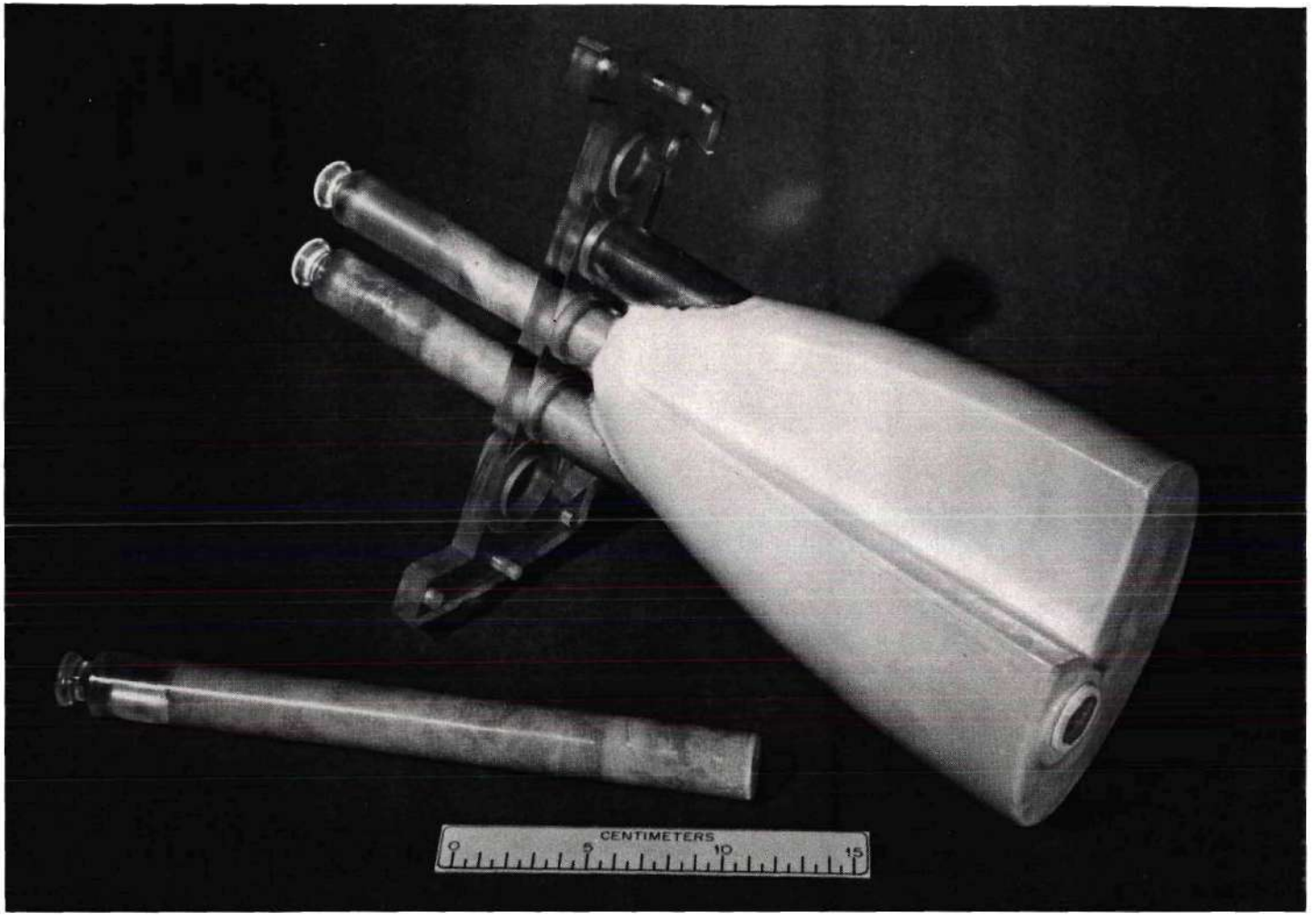

Figure 16. Photograph of Left Lung with Tubes

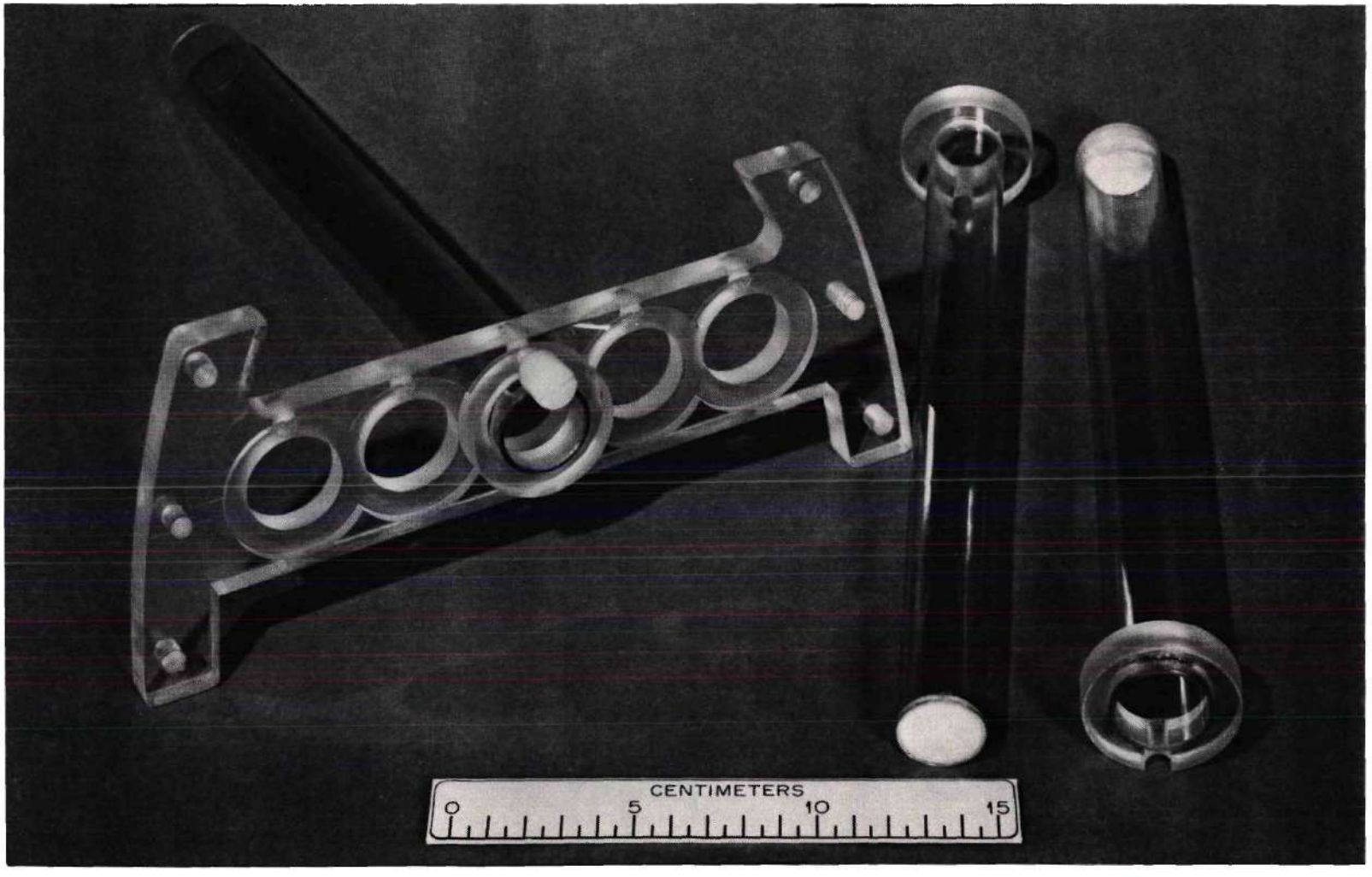

Figure 17. Photograph of Plate for Locating Dosimeters When Lung Is Out. Several Available Tubes Shown.

fill unused locations, and a frame with locating tubes used when data were taken with the lungs out. On an exposure of one lung simulating Rijswijk's geometry, seven locations were available: entrance and exit on the surface of the phantom and 3, 6, 9, 12, and 15 cm deep. The cross section of the phantom through the center of a lung is approximately 18 cm thick. Because of the size of the dosimeters (approximate diameter 2 cm), the locations at 3 and 15 cm depth were unusable when the ribs or lungs were in place. The dosimeters fit snuggly into the lung access holes as well as in the locating tubes used in the frame in Figure 17. This reduced the error in positioning to a small fraction of the total uncertainty in dose.

The requirements of tissue equivalence for neutrons are different from those for photons because it requires matching nuclear densities, not electronic densities. Table 1 lists the percent by weight of the elements for each of the three regions of the mathematical model and its equivalent substitute. This similarity on an element by element basis results in photon mass attenuation and absorption coefficients, and mean free path which agree to better than 5% from 10 keV to high energies. It therefore results in neutron tissue equivalence. The lung and tissue materials were developed particularly for this dissertation (Shonka and McGinley, 1976). The skeleton-equivalent material is that developed by Garry et al. (1975).

Energy Compensated Geiger-Müller Tube

The energy compensated Geiger-Müller (G-M) tube is one of the best available detectors of gamma rays in a mixed-field environment. This device has extremely low neutron sensitivity. It has been observed that when the neutron sensitivity of the photon detector is small, a minimum is

obtained in the overall uncertainty in both the neutron and photon absorbed dose (ICRU, 1977). The principle of the device relies on the fact that appropriate shielding can compensate the energy response of a G-M tube so that each count represents an equivalent absorbed dose regardless of photon energy (Hurst and Wagner, 1958). Two factors are responsible for the low sensitivity of this device to fast neutrons. The first is the fact that as the atomic number increases, the kerma for fast neutrons tends to decrease. This decrease is most noticeable when hydrogen is eliminated--the energy compensated Geiger-Müller tube is constructed with no hydrogen bearing material. The second factor is that, regardless of the initial ionization, pulses from a G-M tube are nearly equal. Hence, the pulse from a heavy ion recoil, which would deposit considerably more dose in tissue than an electron, is given the same weight as an electron released by a photon.

The device used for this work was the Philips micro G-M tube No. 18509. The photon response of this device has been extensively investigated (Wagner and Hurst, 1960). Through improvements in the shield, response to photons is nearly linear from 55 keV photon energy to nearly 5 MeV, and remains within 25% to 8 MeV photon energy (Wagner and Hurst, 1961)(Thorngate and Johnson, 1965). Thermal neutron response is low, 5×10^{9} neutrons/cm^{2} are required to produce the same response as one rad of gamma radiation. This is further reduced to 1.5×10^{12} thermal neutrons/cm^{2} with the addition of a lithium shield which was utilized during this research.

The fast neutron response was reported to be less than 0.14% of the photon response with a maximum at 5 MeV neutron energy, and measurements

indicated the response in this energy range was less than 0.5% (Wagner and Hurst, 1961). At 14 MeV the results are not as conclusive. One measurement indicated a neutron sensitivity of less than 0.5% (Colvett, 1974). However, recent measurements using a coincidence technique based on the associated particle technique demonstrated a sensitivity of 2.47% at 14 MeV (Lewis and Young, 1977). The sophistication of the technique used in this latter experiment led to the adoption of the latter value of 2.47% fast neutron sensitivity at 14 MeV for this research. As a comparison, another detector for photons in a mixed-field environment is the TLD-700 thermoluminescent material whose fast neutron sensitivity has been estimated to be 18% (McGinley, 1971).

The gamma sensitivity of the G-M tube used for this experiment was measured as 4.21×10^3 counts per mrad. This is in good agreement with previous results (Wagner and Hurst, 1961)(Thorngate and Johnson, 1965). The statistical uncertainty in these data was less than 1%. Deadtime of the counting system and detector was measured as 28.8 microseconds, also in good agreement with similar detectors (ICRU, 1977). Calibration was done against an ionization chamber whose calibration was traceable to the National Bureau of Standards. Overall uncertainty in these studies was estimated to be 10%, the major portion being due to the uncertainty stated for the calibration chamber.

Tissue Equivalent Ionization Chamber

A tissue equivalent ionization chamber was used to measure dose in these experiments. A photograph of the device is shown in Figure 18. The chamber has 0.5 mm wall surrounding a nominal 1/2 cc volume. The device is commercially available from the Physical Sciences Laboratory. A loan

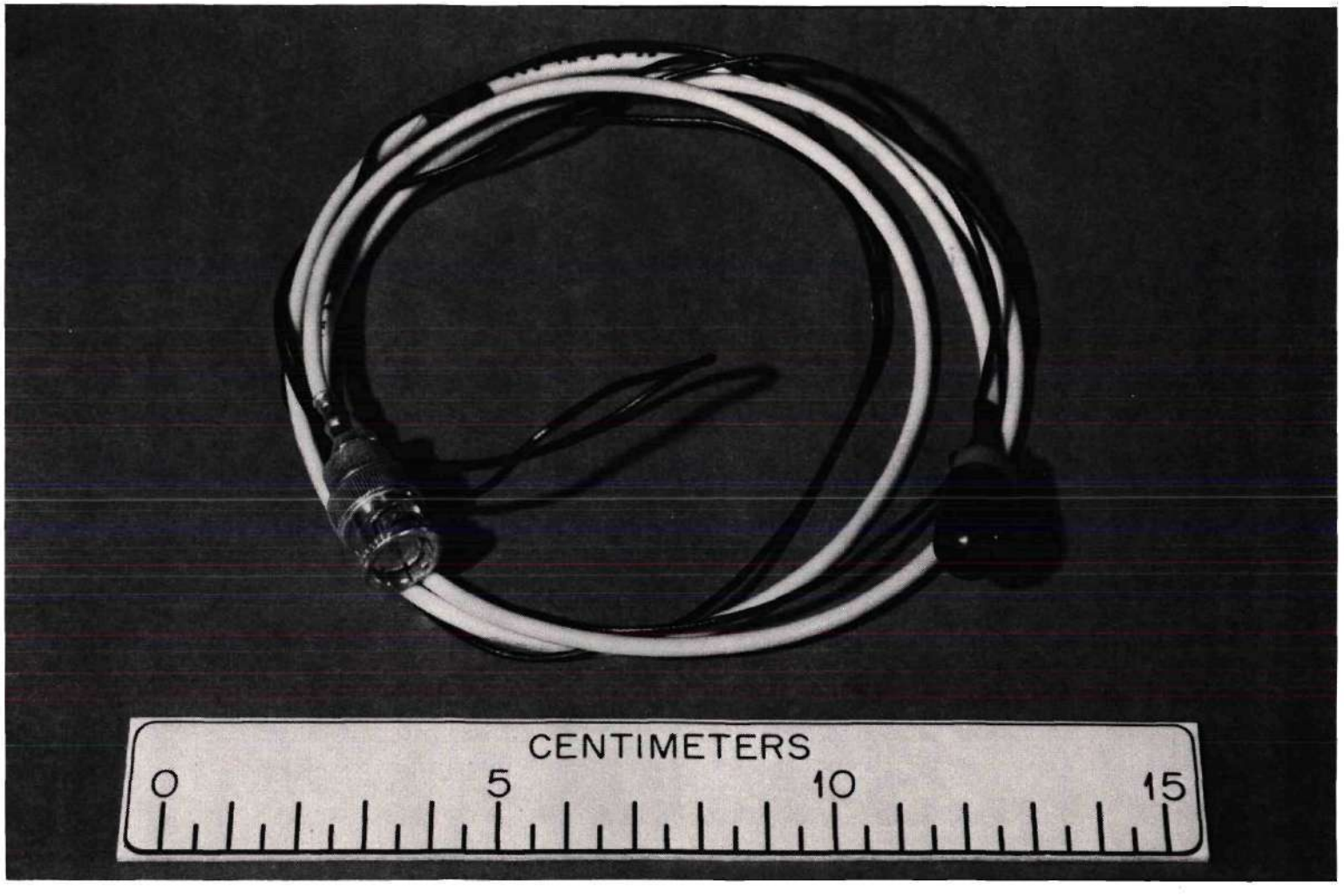

Figure 18. Photograph of Gas-Flow, Tissue-Equivalent Ionization Chamber

of the instrument for the duration of this experiment was graciously arranged by Dr. John Spokas, current director of that laboratory. The geometry as seen from the photograph is cylindrical with a hemispherical end. The chamber is equipped for gas flow and can be pressurized slightly. In the present experiment, a tissue-equivalent gas mixture (Rossi, 1968) flowed through the chamber at atmospheric pressure. The chamber walls are A-150 tissue-equivalent plastic whose precise composition has been the subject of a recent study (Smathers et al., 1977). One result of this study has been a revised value of kerma for A-150 plastic of 6.89×10^{-9} rads-cm^2 at 14.5 MeV neutron energy (ICRU, 1977). Previously, a value of 7.08×10^{-9} rads-cm^2 was used. A close fitting equilibrium cap of 3.5 mm thickness was machined from A-150 plastic. With the cap in place, total wall thickness was 4 mm, adequate for electronic equilibrium for ^{60}Co which was employed for calibration. The dimensions of this cap matched those of the G-M tube with its lithium shield in place, and was employed in the phantom to permit accurate placement of the ion chamber.

A Keithley electrometer model 610C was employed to measure current or charge. This device was modified to permit remote operation by mounting a solenoid on the zero switch. There is an analogue signal available with this device, and it was sent over 200 feet to the control room where a digital voltmeter was used to measure it. The input FET transistors of the electrometer were sensitive to radiation so the electrometer was placed in a lead cave embedded in the concrete shielding wall to reduce its exposure. Approximately 80 cm of low-noise antiphonic cable connected the chamber to the electrometer. This resulted in a system capable of measuring 10^{-13} Coulombs of charge reliably, allowing integration of signal currents as

small as 10^{-15} amperes. This corresponds to a dose of less than 0.5 mrad delivered at 0.25 mrad/min. The chamber exhibited saturation current at applied voltages between 50 and 150 V, so a 90 V battery supply was used for these measurements. Detailed analysis of the data from this chamber is provided in another section; however, two measurements are described below.

The measurement of W, the average energy needed to form an ion pair, is generally performed in a separate apparatus specifically designed for W measurements. The capability of gas flow with this ion chamber permitted a check to be made of the W value for the TE gas employed in these measurements. To do this, two measurements are required. One measurement is made by flowing the TE gas through the chamber. Without altering irradiation conditions, high purity nitrogen is substituted for the TE gas and the current, which is slightly lower, is observed. The dose measured in both circumstances is identical and equating the Bragg-Gray relation for both gases yields

$$S_{N_2}^{TE} \; W_{N_2} \; \frac{I_{N_2}}{\rho_{N_2} \times V} = S_{TE}^{TE} \cdot W_{TE} \cdot \frac{I_{TE}}{\rho_{TE} \times V} \qquad (9)$$

Solving for W_{TE} and replacing constants with appropriate values yields:

$$W_{TE} = 35.1 \times I_{N_2} / I_{TE} \qquad (10)$$

Our measurements indicated a W value of 29.74 ± 0.5 eV/ion pair, a value in good agreement with others published in a recent dosimetry intercom-

parison of fast neutron therapy centers in the United States (Smith et al., 1975).

The chamber employed for these measurements had an effective volume of 0.47 cc, close to its nominal 0.5 cc volume. This was measured by calibrating against ionization chambers whose calibrations were traceable to the National Bureau of Standards.

Tissue Equivalent Proportional Counter

Tissue Equivalent Proportional Counters (TEPC) have found wide application as a means to measure LET or quality of radiation (Rossi, 1968)(ICRU, 1977). The TEPC used for this set of measurements was a 1/2 inch diameter counter available commercially from EG&G. Designated Model LET-SW 1/2, this device has walls constructed of 0.05 inch thick A-150 tissue-equivalent plastic. The device is housed in a gas-tight, thin-walled aluminum shell and has dimensions that are ratios of those first proposed for a fast neutron spectrometer (Benjamin et al., 1968). In this design, field shaping tubes define the electric field eliminating the need for a helical grid about the central wire; a necessity in the original design of the TEPC (Rossi and Rosenzweig, 1955). The device as supplied by the manufacturer is equipped with a quick release vacuum fitting for changing counter gas. Operation of this device as received was unreliable and the TEPC was modified for this work by the addition of a valve. The valve was located to permit direct connection of the pre-amplifier to the counter, which was not possible with the original fitting. This lowered the stray capacitance at the input of the charge sensitive preamplifier and improved the signal to noise ratio.

Two gas mixtures are commonly used with this TEPC. One is methane based and the other substitutes propane for methane (Srdoc, 1970). Srdoc found that a tissue-equivalent gas mixture composed of propane, nitrogen and carbon dioxide improved TEPC performance. Cyclopropane was used with good results in an absolute fast neutron dosimeter operating in a proportional mode (Hurst, 1954). In this experiment, cyclopropane was substituted for propane for use in the TEPC. Two primary benefits occurred: a slight improvement in resolution and a gas whose composition was a closer match to the A-150 tissue-equivalent plastic used in construction of the chamber (Shonka et al., 1975).

To test the new composition, a low-pressure mixing tank was built. The tank was filled with the methane, then with propane, and finally with cyclopropane gas mixtures. The TEPC was filled to pressures simulating a one micron diameter sphere of tissue. A capacitance manometer was obtained to measure the pressure accurately. A change in gain and pressure was observed and was traced to absorption of gas by the A-150 plastic.

The absorption properties of tissue-equivalent plastic had been studied previously (Marshall et al., 1964). His work showed that different gases are absorbed by A-150 plastic at different rates and to different saturation levels. To avoid these problems, a protocol for filling was established which permitted saturation in the A-150 plastic of the various gas components. The shift in gain and pressure was eliminated with this procedure. The procedure involved evacuating the chamber with a diffusion pump for several days to remove adsorbed oxygen and other contaminants, followed by repeated fillings to the working pressure for several days (Shonka et al., 1975).

The Paired Equations

All neutron fields employed for radiotherapy have a photon component. The ICRU has advised that the absorbed dose should be separated into its photon and neutron components (ICRU, 1977). Two dosimeters are required to do this. In all systems commonly used, one detector has essentially equal sensitivity to both neutrons and photons while the other detector has a lower sensitivity to neutrons than its photon response. The paired equations are used to separate the photon and neutron doses from the measurements made with the two dosimeters. Using the notation of the ICRU (ICRU, 1977):

$$R_T = k_T D_N + h_T D_G \tag{11}$$

$$R_u = k_u D_N + h_u D_G \tag{12}$$

where

T = subscript designating dosimeter approximately equally sensitive to neutrons and photons (TE ion chamber)

u = subscript designating dosimeter more sensitive to photons (energy-compensated G-M tube)

D_G = absorbed dose due to photons

D_N = absorbed dose due to neutrons

R_u, R_T = quotient of response of detector by calibration photon sensitivity

k_u, k_T = ratio of sensitivity of detector to neutrons by calibration photon sensitivity

h_u, h_T = ratio of sensitivity of dosimeter to photons by calibration photon sensitivity

If one multiplies these equations by the sensitivity of each detector to the photons used for calibration, it is obvious that the response of the T detector equals the neutron dose times its sensitivity to neutrons plus the photon dose times its sensitivity to photons. A similar statement can be made for the U detector. This work utilized the equations in this latter form. Thus, four parameters were needed to analyze the data from the TE ion chamber (T detector) and the Phil (U detector), that is, their sensitivities to photons and neutrons, respectively. The sensitivities to photons for both detectors were determined by calibration in air one meter from a ^{60}Co photon source. The exposure was measured by ionization chambers whose calibrations were traceable to the National Bureau of Standards.

The Phil required an adjustment of its calibration to account for the fact that its photon response increases slightly with energy (Thorngate and Johnson, 1965). In a tissue-equivalent medium, most of the photon dose from a neutron flux is delivered by photons from the hydrogen capture reaction (Auxier, Snyder and Jones, 1968). This yields a photon of 2.2 MeV in energy, with a mean free path of more than 20 cm in tissue. For this work, it was noted that Thorngate and Johnson observed the response of the Phil was 4% greater for this 2.2 MeV gamma radiation than for the ^{60}Co gammas; thus the calibration coefficient increased from 4.21×10^6 counts per rad to 4.387×10^6 counts per rad.

The neutron sensitivity of the Phil at 14 MeV was recently measured

to be 1.235 x 10^5 counts per rad (Lewis and Young, 1977). This value was used without adjustment resulting in the following equation

$$R_u = 1.235 \times 10^5 D_N + 4.387 \times 10^6 D_G \quad (13)$$

Calibration of the TE chamber in the same ^{60}Co field yielded 5.501 rads per nanocoulomb. Because no significant variation in response occurs with this chamber over wide photon energies, this value was not adjusted.

The neutron response of TE ionization chambers was recently reviewed by Barschall and Goldberg (1977) who pointed out two techniques to calibrate a detector. The first, like the Phil calibration discussed above, was based on fluence. No suitable facility was available for this calibration. The other, more common technique is based on the Bragg-Gray relation. Stated in the MKS system of units,

$$E/Q_i = 100 \cdot W_i/e \cdot S_i/M \quad (14)$$

where

E = dose in rads in TE plastic

Q_i = charge collected in Coulombs

W_i = energy in joules to create ion pair

e = charge of electron in Coulombs

S_i = mass stopping power ratio for wall to gas

M = mass of gas in kilograms

Barschall and Goldberg gave the following values for 14 MeV neutrons:

W_i/e = 31.4 eV $\qquad$ S_i = 0.995

Using the photon calibration to compute the mass of gas involved, and correcting the dose in TE plastic to that of tissue by multiplying by the ratio of kerma yields a fast neutron sensitivity of 5.487 rads per nanocoulomb for this chamber. This yields the other equation as:

$$R_T = 0.1822\, D_N + 0.1818\, D_G \qquad (15)$$

Equation (13) together with equation (15) form the paired equations used for analyzing data from the Phi1 and TE chamber.

CHAPTER V

RESULTS

Homogeneous Depth Dose Distributions

Central axis depth dose was determined at seven detector locations in the phantom filled with TE liquid. These locations were approximately 3 cm apart. Table 4 summarizes these results for the homogeneous case.

Table 4. Neutron and Gamma Dose Measured in the Homogeneous Phantom

Detector Location	Approximate Depth (cm)	Neutron Dose (rads/ neutron)	Relative Neutron Dose (%)	Gamma Dose (rads/ neutron)	Relative Gamma Dose (%)
1	0.4	2.99×10^{-13}	100	2.00×10^{-14}	100
2	3.4	2.34×10^{-13}	78	1.86×10^{-14}	93
3	6.4	1.60×10^{-13}	54	1.48×10^{-14}	74
4	9.5	1.03×10^{-13}	44	1.21×10^{-14}	61
5	12.5	0.64×10^{-13}	21	0.93×10^{-14}	46
6	15.5	0.37×10^{-13}	12	0.69×10^{-14}	34
7	18.6	0.21×10^{-13}	7	0.47×10^{-14}	24

Each measured value represents the average of at least five separate measurements. The experimental standard deviation ranged from 1 to 2.5% for the Phil, and from 1.5 to 5.2% for the TE ion chamger. If the only source of error were statistical, these errors would result in uncertainty in the

neutron and gamma doses ranging from 2 to 6%.

The uncertainty in position was less than 1 mm radially by virtue of use of the laser backlighting technique. Uncertainty in position along the depth dose axis was due to the uncertainty in measuring the distance and the uncertainty in the center of ionization in the chamber, since reproducibility of better than 1% was achieved by the locator tubes shown in Figure 17. The errors in measuring the depth ranged from less than 0.1 mm at position 1 where the dosimeter abutted the collimator (machined to a tolerance of ± 0.02 mm), to approximately ± 0.5 mm at position 7. When a cylindrical ionization chamber is exposed to a beam of fast neutrons, a displacement correction is required because the point of measurement is shifted from the center of the chamber toward the neutron source. The displacement for 14 MeV neutrons in a cylindrical chamber is between 3r/4 and r where r is the inner radius of the chamber (ICRU, 1977). In the present research, the center of ionization was presumed to be shifted by r, that is, the inner wall nearest the accelerator was used as the point for all depth measurements. Overall the contribution to total error in the measurements from positional uncertainty from these two factors was judged to be in the range of from 1 to 2%.

Obviously, the experimental uncertainty expressed above is not the total for these values of dose. To compare these results in an absolute manner against calculations, the uncertainty in the parameters h_T, h_u, k_T, and k_u of the paired equations has to be evaluated. The sensitivities of the TE ion chamber and Phil to photons are h_T and h_u, respectively. A ^{60}Co source of photons was used for calibration. The field was measured by ion

chambers whose calibration was traceable to the National Bureau of Standards. The dominant uncertainty in h_T and h_u was the 10% uncertainty quoted for the calibration of these ion chambers by the supplier (Victoreen, 1977). Slight additional uncertainty in h_u can be attributed to its non-linear energy response. The calibration for ^{60}Co was adjusted to the 2.2 MeV photon ($^1H(n,\gamma)^2H$), the most abundant photon produced in neutron interactions in tissue. Other photons are produced, however, resulting in slight additional uncertainty in h_u. The uncertainty in k_u was extracted from the literature (Lewis and Young, 1977). The quoted accuracy of 8% was increased to 10% to account for the fact that the G-M tube in that work was similar, but not identical to the one used in this work, and their quoted value of 1.235×10^5 counts per rad of 14 MeV neutrons differed from previous results.

The sensitivity of the TE ion chamber in nanocoulombs per rad of fast neutrons is k_T. To calculate k_T, this work relied on parameters recently evaluated by Barschall and Goldberg (1977). In that work, the authors stated that the uncertainty in k_T is dominated by the uncertainty in W (estimated at 7%). They also stated that it was difficult to know how to combine all the uncertainties involved in determining k_T. Thus, an uncertainty of 10% was assigned to k_T, reflecting the fact that uncertainty in W dominates, but other factors do contribute.

If all errors are propagated through the expressions for the neutron and photon doses obtained from the paired equations, one standard deviation for either the neutron or photon dose is approximately 25%. This is dominated by the uncertainty in calibration. This is the uncer-

tainty for the absolute value of dose. If one considers the relative depth dose, one standard deviation ranges from 4 to 8% since all values are arbitrarily normalized to 100% at the depth of maximum dose.

Figure 19 compares these results with selected previous work. The Monte Carlo calculations of Jones et al. (1971) were corrected from infinite SSD (parallel entry of neutrons into phantom) to an SSD of 45 cm by the inverse square law. McGinley observed that, in correcting from one SSD to another, only the primary radiation should be adjusted (McGinley, 1973). The amount of secondary radiation produced as a function of depth per unit fluence remains the same regardless of SSD. McGinley's technique for adjusting one SSD to compare with another was used for all comparisons in the present research. The slight difference observed after adjusting Jones' results to an SSD of 45 cm can be attributed to the differences in the model used in the calculations. These differences include cylindrical geometry as opposed to the ellipse used in the measurements and 5 cm circular beam assumed in the calculations as opposed to the 6 x 8 cm beam used experimentally. McGinley (1971) has shown a loss in penetration with decreasing field size at 14 MeV. Thus, at shallow penetration, the smaller field used in the calculations resulted in a lower dose. At deep penetration, a cylindrical geometry offers more tissue medium for backscattering of the scattered component of the beam. These two competing effects cause these two curves to cross.

Also shown in Figure 19 are experimental results by McGinley corrected to 45 cm SSD from 125 cm and normalized to the results from this dissertation (McGinley, 1971). Also shown are results from Rijswijk and

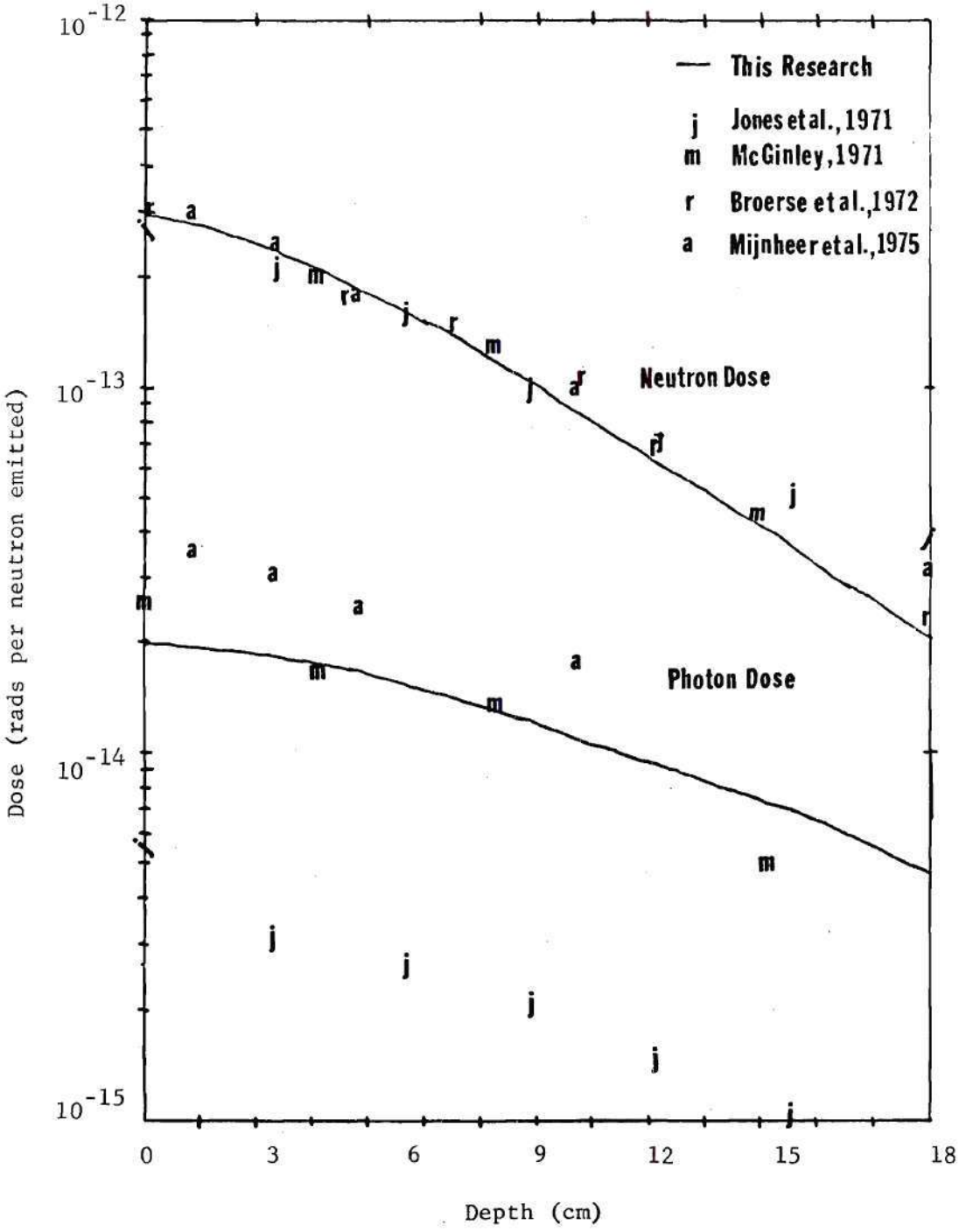

Figure 19. Comparison of Depth Dose Distributions for the Homogeneous Soft Tissue Phantom

Amsterdam using similar geometries (Broerse, Broers-Challiss, and Maruyama, 1972)(Mijnheer, Broers-Challiss, and Broers, 1974). The results from the work of Mijnheer et al. are for a 30 cm cube and reflect increased scattering material available at depth. Thus, the Dutch work agrees well at shallow penetration and at greater depths gradually exceeds values found in the present work. In all cases, agreement is well within the standard deviation reported by the respective authors. Moreover, agreement between the calculations of Jones et al. and this work was achieved without arbitrarily normalizing either result.

Heterogeneous Depth Dose Distributions

Depth dose measurements were made for three heterogeneous phantoms. These were the elliptic phantom filled with lung and TE liquid, then filled with the skeleton and TE liquid, and the complete phantom with lung, skeleton and TE liquid. Calculations of depth dose were made for the complete phantom. In the measurements, only five of the detector locations were available, since both the skeleton and lungs occupied portions of detector locations 2 and 6. The five remaining locations were identical to those reported for the homogeneous phantom, and the same correction for uncertainty in position was applied for these cases. Again this resulted in an increase in the error value for dose of 1 to 2%. As was stated in the homogeneous results, uncertainty in both calibration and W for the ion chamber dominated the overall error. The same values discussed in that section apply here as well, resulting in one standard deviation of 25% for either the measured neutron or photon dose.

Lung in the Tissue-Equivalent Phantom

The results for the phantom with only the lungs in place are presented in Table 5.

Table 5. Neutron and Photon Dose Measured in the Phantom with Lungs in Place

Detector Location	Approximate Depth (cm)	Neutron Dose (rads/ neutron)	Relative Neutron Dose (%)	Gamma Dose (rads/ neutron)	Relative Gamma Dose (%)
1	0.4	3.02×10^{-13}	100	1.65×10^{-14}	100
3	6.4	1.56×10^{-13}	52	1.36×10^{-14}	82
4	9.5	1.31×10^{-13}	43	1.13×10^{-14}	68
5	12.5	1.02×10^{-13}	41	0.91×10^{-14}	55
7	18.6	0.54×10^{-13}	18	0.54×10^{-14}	33

The major change observed in comparing results from Tables 4 and 5 is the increased transmission through the phantom when the low density lungs are in place. The neutron doses with and without lungs agree to within 1% at the front of the phantom (location 1). The neutron dose more than doubles at the rear of the phantom with the lung in place due to the decreased attenuation.

While small differences do occur with and without the lung in place, the neutron-induced photon dose agrees to within 20% for the two cases. The neutron-induced photon dose in Table 5 ranges from 5% of the total dose, i.e. $(n+\gamma)$, at the front of the phantom to 10% at the rear. This is in general agreement with results published previously (McGinley, 1971), (Broers et al., 1972) and (Mijnheer et al., 1974).

Depth dose data for the phantom with the lung in place are shown in Figure 20. The data of Rijswijk for virtually the same geometry were normalized to those of this work and plotted on this same graph. In general, the agreement is quite good. Also shown in the same plot are data from the clinical trial in Amsterdam (Mijnheer et al., 1974). This latter work utilized a cubical phantom rather than the elliptic geometry used in this dissertation. As in the case of the homogeneous phantom, the depth dose exhibits somewhat greater penetration in a cubical geometry because more tissue-equivalent material was available to scatter neutrons back into the beam.

The results from McGinley's dissertation are shown also in Figure 20 (McGinley, 1971). Several major corrections were required to obtain the general agreement shown. The largest correction occurred in changing from an SSD of 125 cm to one of 45 cm but this factor alone was unable to reconcile differences in results. McGinley used an 18.4 x 18.4 cm beam at 125 cm SSD. To normalize his data approximately to the 6 x 8 cm beam used here, his results for various beam sizes in the homogeneous phantom were scaled as a function of depth. The number obtained was multiplied by the depth dose corrected to 45 cm SSD. The resultant numbers were then arbitrarily normalized at the front of the phantom to the results from this dissertation. As in the case of the homogeneous phantom, all data then agree within the confidence limits specified by the respective authors. McGinley also compared his work with that of Wilkie who did broad-beam Monte Carlo calculations in the chest region (Wilkie, 1970). Comparisons with that work are made for those of the complete phantom later in this section.

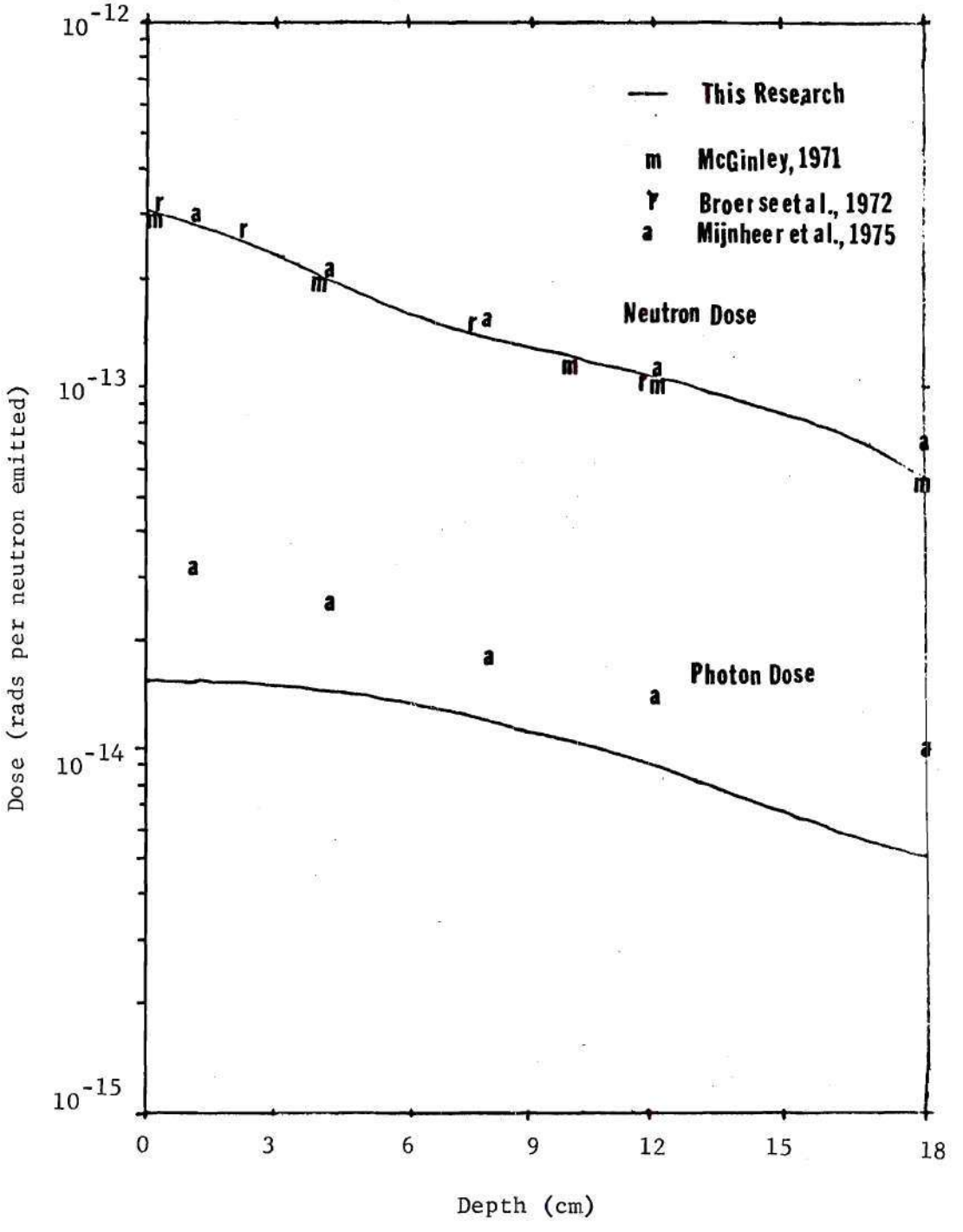

Figure 20. Comparison of Depth Dose Distributions in the Heterogeneous Phantom with Lung and Soft Tissue

Bone in the Tissue-Equivalent Phantom

In an attempt to separate the effects of bone and lung tissue on depth dose, measurements were made in the phantom with the skeletal system appropriately located in the tissue-equivalent fluid of the phantom. The measurements of the fast neutron and gamma dose are summarized in Table 6. Experimental uncertainty ranged from 1 to 2% for the Phil and from 2 to 3% for the ion chamber.

Table 6. Neutron and Gamma Dose Measured in the Phantom with the Skeletal System in Place

Detector Location	Approximate Depth (cm)	Neutron Dose (rads/ neutron)	Relative Neutron Dose (%)	Photon Dose (rads/ neutron)	Relative Photon Dose (%)
1	0.4	2.89×10^{-13}	100	2.15×10^{-14}	100
3	6.4	1.51×10^{-13}	52	1.51×10^{-14}	70
4	9.5	0.99×10^{-13}	34	1.18×10^{-14}	55
5	12.5	0.60×10^{-13}	21	0.91×10^{-14}	42
7	18.6	0.19×10^{-13}	7	0.49×10^{-14}	23

McGinley made measurements with a cylinder of bone equivalent plastic in a phantom (McGinley, 1971). The cylinder diameter was 4 cm which greatly exceeded the size of bones of the skeletal system in the phantom employed for this work. McGinley drew two conclusions based on his measurements. First, there was a 7% increase in dose immediately in front of bone which he theorized was due primarily to backscattering from bone. The results from this dissertation neither support nor deny this conclusion because no increase in neutron dose in front of bone was observed in

these measurements. The ribs are 0.5 cm thick in the phantom, and in addition are interspersed with tissue. Thus a factor of at least 1/16 should apply and an increase of less than 0.5% would be expected. In fact, a decrease of 3% instead of an increase is observed but this is within the experimental error and hence may show general agreement with McGinley's data.

McGinley's second conclusion was that the depth dose behind bone is essentially the same as in the homogeneous case. While the present measurements show a decrease of 4 to 5% in dose with depth when bone was present, this is within the experimental uncertainty and McGinley's conclusion is neither supported nor denied.

Lung and Bone in the Tissue-Equivalent Phantom

Both measurements and calculations were performed in this study for the full heterogeneous phantom and the results are given in Table 7.

Table 7. Measurements and Calculated Values of Depth Dose in the Heterogeneous Phantom

Detector Location	Measurements		Calculations	
	Neutron Dose (rads/neutron)	Gamma Dose (rads/neutron)	Neutron Dose (rads/neutron)	Gamma Dose (rads/neutron)
1	2.96×10^{-13}	2.05×10^{-14}	2.75×10^{-13}	0.39×10^{-14}
2			1.88×10^{-13}	0.31×10^{-14}
3	1.38×10^{-13}	1.38×10^{-14}	1.22×10^{-13}	0.26×10^{-14}
4	1.26×10^{-13}	1.08×10^{-14}	0.91×10^{-13}	0.27×10^{-14}
5	0.99×10^{-13}	0.91×10^{-14}	0.96×10^{-13}	0.15×10^{-14}
6			0.65×10^{-13}	0.20×10^{-14}
7	0.58×10^{-13}	0.52×10^{-14}	0.73×10^{-13}	0.17×10^{-14}

The experimental uncertainties ranged from 1 to 2% for the Phil and from 2 to 4% for the TE ion chamber. The same uncertainties in position and calibration as were discussed in previous sections apply here as well. When the errors are propagated through the expressions for the neutron and gamma doses, the resultant uncertainty for the neutron and photon doses is approximately ± 5% in relative terms and ± 25% in absolute value.

The uncertainty in calculated values is expressed as a coefficient of variation, or the standard deviation of the calculated value divided by the mean. In the calculated values of neutron dose, the coefficient of variation ranged from ± 15% in the front of the phantom to ± 25% in the back. Thus the calculated neutron dose shows general agreement with the measured value, always within the standard deviation of either technique.

Another point that can be made is that the large coefficients of variation found for the depth dose data were due in part to the small detector size in the phantom. For the calculation, a 1 cm diameter sphere centered about each of the seven detector locations was used as the volume to sum interactions for dose. Choice of a larger volume could have reduced the large coefficients of variation found in the depth dose date but would have reduced spatial resolution.

The calculated photon dose differs substantially from the measured values. Calculated values of photon dose had coefficients of variation ranging from 50 to 70% and with such large uncertainty, little trust can be placed in the calculated photon dose except as to order of magnitude. However, it is interesting to note that the calculated value is substan-

tially less than the measured photon dose. This probably reflects the inadequate model assumed for the source term in the calculation. The source was assumed to be a pure neutron emitter, and neutrons were permitted to impinge on the phantom only when their flight paths transited the collimator aperture. In the actual experiment, however, photons were produced by inelastic and capture reactions not only in the phantom but also in the collimator and shield. Results for an identical collimator at Rijswijk indicated that 10 cm from the bean axis the photon dose in air near the collimator amounted to 4% of the total dose in the beam (Broers et al., 1972). From this figure it can be deduced that over half of the photon dose was neglected by the assumptions used for the source term of the Monte Carlo code. These assumptions also neglected those neutrons that passed through the steel in the collimator and into the phantom but this made a somewhat smaller contribution. Thus, the photon dose calculation suffered not only from large uncertainty, but in all probability was in error due to inadequacy of the chosen model.

In related calculations, Wilkie (1970) presented data from a broad-beam exposure of a chest to 14 MeV neutrons. The chest model used was a cross section in the thoracic region extended in the vertical direction. Overall, a good deal of similarity exists between the phantoms used in his study and the one under investigation here, but several adjustments need to be applied to compare his work with the values presented here.

The major adjustment is for inverse square loss. However, making this adjustment alone does not reconcile the two sets of data. Using

McGinley's data showing the effect of beam size on central axis depth dose, one can make a crude correction from Wilkie's broad-beam to a 7.5 x 7.5 cm beam at the front surface of the phantom. Wilkie presented his data in relative terms. However, if his data are normalized as indicated above, to the dose in front of the phantom, agreement within the quoted accuracy of each author is obtained.

The neutron and photon depth doses for the four experimental conditions are shown in Figure 21. The figure shows a plot of depth dose for the homogeneous and each of the three heterogeneous phantoms. With lung in the phantom, the increased transmission from the low density lung results in higher neutron and photon dose at the back of the phantom. The effect of skeletal tissue is more subtle, but there appears to be a slight shadowing effect behind bone. Any increase in dose in front of bone appears to be due to photons.

Dose to Various Organs

The Monte Carlo code developed for this dissertation was programmed to calculate average dose in 97 organs of the body, but there is considerable duplication in these 97 organs. For example, left lung, right lung, both lungs, trunk and total body are all considered to be separate organs. Energy deposited in the left lung is tallied in four of these five organs simultaneously. Table 8 presents the neutron dose to all organs with dose exceeding 10^{-15} rads per neutron emitted from the target, and with coefficient of variation less than 30%. Not included in that table is dose to the head which received less than 0.25% of the dose delivered to the irradiated lung, and the testes which received virtually no neutron exposure

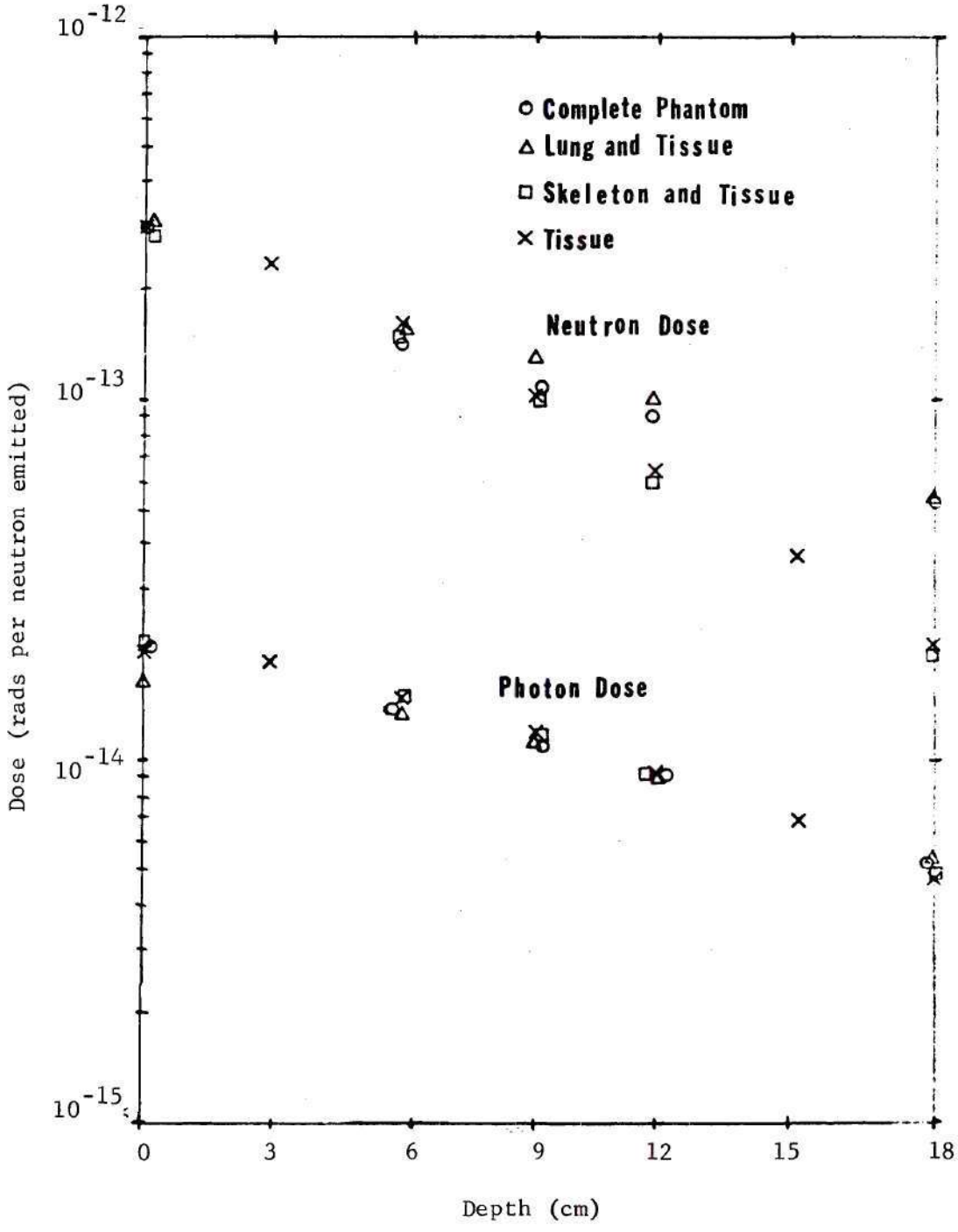

Figure 21. Neutron and Photon Depth Dose Distributions for All Four Experimental Phantoms: Homogeneous; Lung and Soft Tissue; Skeleton and Soft Tissue; and Lung, Skeleton and Soft Tissue

Table 8. Calculated Dose to Various Organs

Organ	Neutron Dose (Rads per n/cm^2)	Coefficient of Variation (%)	Photon Dose (Rads per n/cm^2)	Coefficient of Variation (%)	Organ Mass (g)
Left Adrenal	1.99×10^{-15}	29	2.41×10^{-14}	50	7.75
Adrenals	1.30×10^{-15}	33	1.77×10^{-14}	40	15.5
Stomach	1.34×10^{-15}	13	2.55×10^{-14}	16	150.0
Stomach Contents	1.03×10^{-15}	10	2.56×10^{-14}	13	247.0
Heart	5.42×10^{-15}	4	6.69×10^{-14}	5	595.0
Left Lung	7.16×10^{-14}	2	1.19×10^{-13}	5	500.0
Lungs	3.61×10^{-14}	2	6.73×10^{-14}	5	999.0
Red Marrow in Ribs	9.16×10^{-15}	3	3.64×10^{-14}	6	153.0
Red Marrow in Scapulae	4.28×10^{-15}	7	2.57×10^{-14}	12	72.0
Red Marrow in Middle of Spine	1.62×10^{-15}	5	2.82×10^{-14}	7	212.0
Red Marrow in Middle of Phantom	4.23×10^{-15}	2	2.89×10^{-14}	4	489.0
Red Marrow	1.42×10^{-14}	2	1.17×10^{-14}	4	1500.0
Yellow Marrow in Ribs	9.16×10^{-15}	3	3.64×10^{-14}	6	201.0
Yellow Marrow in Scapulae	4.28×10^{-15}	7	2.57×10^{-14}	12	24.0
Yellow Marrow in Middle of Spine	1.62×10^{-15}	5	2.82×10^{-14}	7	70.5
Yellow Marrow in Middle of Phantom	6.60×10^{-15}	3	3.25×10^{-14}	4	313.0
Yellow Marrow	1.48×10^{-15}	2	9.77×10^{-15}	4	1500.0
Pancreas	1.07×10^{-15}	19	2.88×10^{-14}	23	60.3

Table 8. Concluded

Organ	Neutron Dose (Rads per n/cm^2)	Coefficient of Variation (%)	Photon Dose (Rads per n/cm^2)	Coefficient of Variation (%)	Organ Mass (g)
Ribs	9.16×10^{-15}	3	3.64×10^{-14}	6	1030.0
Scapulae	4.28×10^{-15}	7	2.57×10^{-14}	12	302.0
Spine	1.06×10^{-15}	5	2.02×10^{-14}	6	1320.0
Skeleton	1.22×10^{-15}	2	9.12×10^{-15}	3	10500.0
Trunk Skin	3.76×10^{-15}	4	1.48×10^{-14}	8	1370.0
Total Skin	1.85×10^{-15}	4	7.57×10^{-15}	8	2790.0
Spleen	2.21×10^{-15}	10	2.89×10^{-14}	15	174.0
Thymus	1.08×10^{-15}	38	3.31×10^{-14}	31	24.8
Trunk Soft Tissue	2.64×10^{-15}	1	1.68×10^{-14}	2	30000.0
Total Soft Tissue	1.64×10^{-15}	2	1.07×10^{-14}	2	48500.0
Trunk	3.22×10^{-15}	1	1.80×10^{-14}	1	42700.0
Total Body	1.98×10^{-15}	1	1.14×10^{-14}	1	69880.0

and only a slight photon dose, which itself was subject to a 70% coefficient of variation because of the distance and small size.

Photon exposures to the same organs are also listed in Table 8. Examination of this table points out the fact that outside the beam the dose deposited is totally dominated by the photon component. It is important to realize that this table underestimates the photon dose since the source routine was not programmed to generate photons produced in the collimator and shield.

LET Distributions in the Heterogeneous Phantom

The Monte Carlo code was used to calculate the fraction of dose in each of 12 broad LET bands at seven detector locations listed in previous sections. The calculation of dose as a function of LET imposed a sizable time demand on the computer. Cross sections for each interaction were needed, and for a given interaction the energy of all products was computed to be stored as a function of LET. Because of the time constraints, relatively few neutron histories were tallied. Given the small detector site size, a sphere of radius 1 cm, it was inevitable that large statistical fluctuations would occur. Because of these factors, Table 9 lists only the LET for three locations: front, midpoint, and back. The coefficients of variation ranged from 15 to 25% for the values in front, from 25 to 30% for the midpoint, and from 30 to 65% for the rear. As such, these figures are useful only to give general trends.

Several corrections need to be made to compare with the work of Jones and co-workers (Jones et al., 1971). As in the case of dose, the fraction of dose in each LET interval needs to be corrected for SSD. In

Figure 9. Average Dose in Various LET Ranges as Calculated for the Heterogeneous Phantom

Detector Site	LET (keV/μ)											
	0-3.5	3.5-7	7-15	15-25	25-35	35-50	50-62.5	62.5-75	75-87.5	87.5-100	100-200	200-
Front	0.014*	0.609	0.542	0.215	0.084	0.067	0.045	0.054	0.054	0.051	0.245	0.640
Middle	0.032	0.134	0.078	0.049	0.038	0.036	0.026	0.025	0.005	0.006	0.113	0.085
Back	0.008	0.311	0.035	0.048	0.055	0.042	0.023	0.020	0.025	0.022	0.088	0.020

*rads x 10^{-13}/neutron emitted.

addition to this, Jones and co-workers were concerned with a homogeneous medium, tissue. In the 18 cm thick cross section of chest used here, the central 13 cm were occupied by lung which is one third the density of tissue. Hence the changes one observes are due to the equivalent of roughly 9 cm of unit density tissue. One would not expect the changes to be as significant as those which occur after 18 cm of unit density tissue. Even with the large coefficient of variation for each of those dose figures, there is still crude agreement with Jones' calculation. In general, these data indicate a slight decrease with phantom depth in that fraction of the dose delivered at LET's between 15 and 100 keV/μ. The dose in this range of LET is due primarily to protons. Beyond this, little can be deduced from the calculations. These calculations are in general agreement with other results at 14 MeV which also showed the decrease in dose deposited by low energy protons produced by collimated neutrons (Paretzke et al., 1972). Major effects other than the one observed have not been reported to this author's knowledge. Thus the calculations successfully predicted changes in LET observed by most other authors.

LET measurements were made in the heterogeneous phantom. Spectra were obtained at the front, middle and back of the phantom with the lungs and skeletal structure in place. A one micron diameter sphere of tissue was simulated by the Benjamin chamber previously described. Using the cyclopropane gas developed for this work, a one micron sphere of tissue is simulated with a gas pressure filling of 3.43 cm. In order to compare changes occurring with depth in the phantom, the accelerator was run until approximately one rad was deposited on the chamber. Approximately 6×10^{12} neutrons for the exposure at the front and 3×10^{13} total neutrons

at the rear of the phantom were required to deposit one rad.

Figure 22 shows the spectra for the three sets of data. Heintz has suggested that if data are presented on a semi-log plot, then displaying $Y^2N(Y)$ (where Y is the event size and N(Y) the number of events) results in a display where the area under the curve is proportional to the dose (Heintz et al., 1971).

As can be seen from the figure, there is a definite loss with increasing depth in that fraction of dose deposited in the interval of LET from 30 to 80 keV/μ. This loss is in the same range of LET as the loss observed from the calculations; however, the magnitude of the loss is significantly greater in the measured spectrum. These results are similar to those reported by Paretzke and support his conclusion that a collimator produces a low energy tail in the initially monoenergetic neutron spectrum. This low energy component preferentially scatters out of the main beam, gradually hardening the neutron spectrum.

An attempt was made to compare the calculated LET spectrum to the measured spectrum in an absolute fashion. Previous results have compared the two methods in a relative fashion by normalizing both curves to the same total area (Paretzke et al., 1972). The attempt to compare the calculated and measured LET spectra failed in part because no correction could be made for dead time losses in the multichannel analyzer used to collect the data. More experimental problems complicated data collection. On the long accelerator runs necessary to irradiate the chamber to 1 rad, the accelerator would overload periodically in an "arc over." The count rate on the neutron channel was observed to increase dramatically during

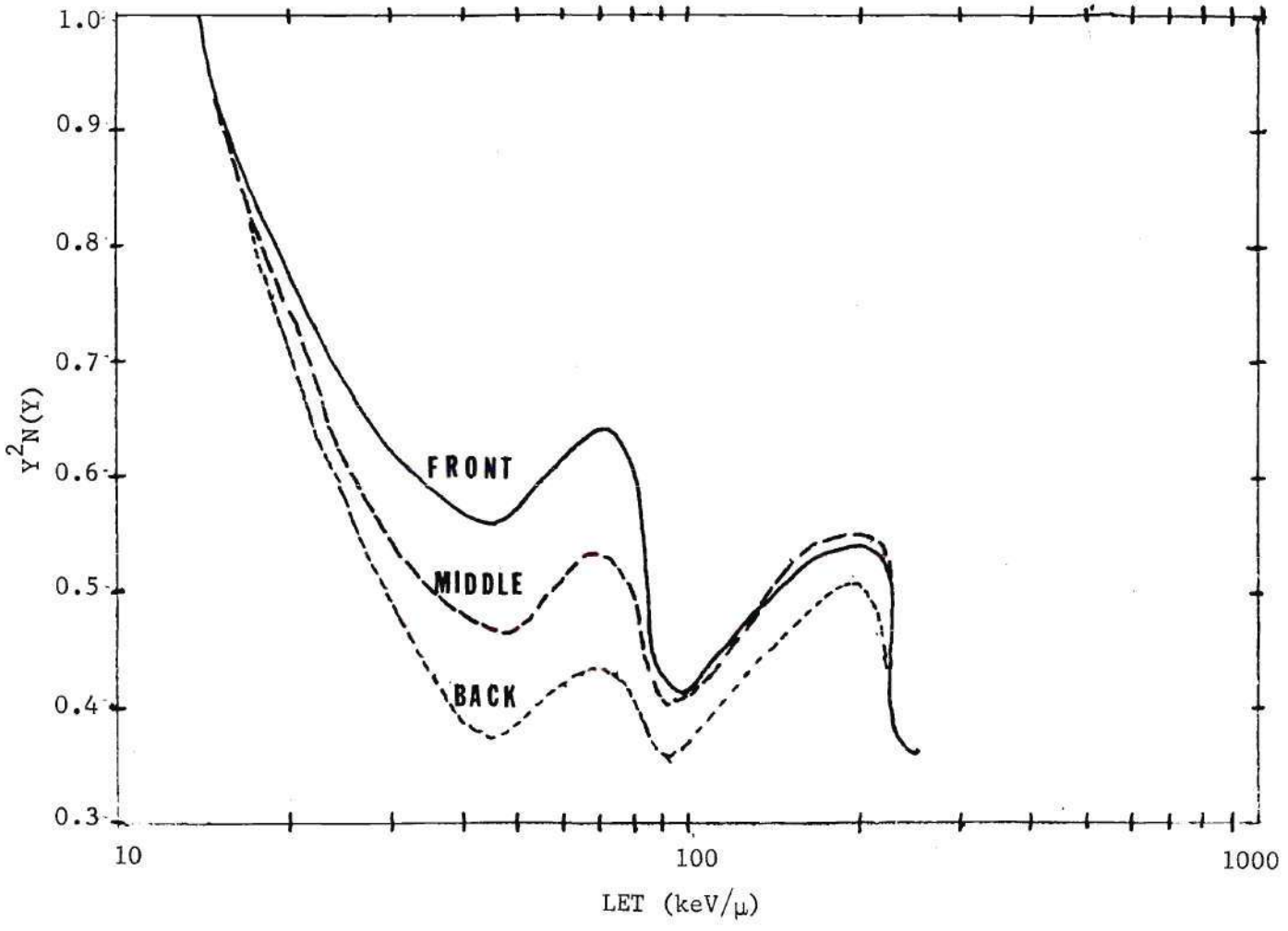

Figure 22. Measured LET Spectra as a Function of Depth in the Heterogeneous Phantom with Lung, Skeleton, and Soft Tissue

an arc over, and more erroneous counts accumulated on the neutron channel as the machine was returned to steady-state operation.

If the experimental difficulties had been overcome, it is doubtful that an exact match would have occurred. This is due to two main reasons. First, the neutron spectrum assumed for the calculation did not match the experimental one in that, in the calculation, no low energy neutrons were produced in the collimator. This point will be further explained in the section dealing with neutron spectrum calculations. The second reason why it is doubtful that an exact match could be made is due to the fact that the A-150 plastic used for the proportional counter inverts the carbon to oxygen ratio present in soft tissue. Paretzke concluded that this difference would alter the LET spectrum between 40 and 260 keV/μ with a pronounced peak at 70 keV/μ.

Neutron Spectra Distributions in the Heterogeneous Phantom

Available output from the Monte Carlo code included neutron spectra at the same detector locations as specified for dose and LET. Thus, neutron spectra were tallied at each of the seven sites specified in the previous sections. The coefficient of variation was not calculated for the neutron spectra generated by the code. The code was inefficient relative to other general purpose Monte Carlo codes due to the time demand of calculating LET. Because it was inefficient and to reduce computation cost, a small number of neutron histories was averaged. It was anticipated that a large coefficient of variation could result, so large energy bandwidths were chosen to minimize the variation.

Table 10 shows the results of the calculations along with the energy intervals used for averaging spectra. The energy intervals corresponded to those used in storing cross sections, and reflect the fact that cross sections tend to vary linearly with lethargy rather than energy. A bar graph of the six highest energy groups is shown in Figure 23. Spectra in the front, midplane, and back of the phantom are shown. The plotted data show a slight trend toward softening of the neutron beam with depth as one might expect.

Measurements for 14 MeV neutrons under broad-beam irradiation conditions have confirmed the expected softening of the initially monoenergetic neutron beam with increasing depth (Hannan et al., 1973). Under collimated conditions, other Monte Carlo calculations indicate that lower-energy neutrons are preferentially scattered out of the beam (Paretzke et al., 1972). These investigators attempted to differentiate between an actual collimator and an ideal aperture. Scattering in the collimator itself results in a beam with a low energy neutron component and an appreciable gamma component. The spectrum then hardens with increasing depth due to the narrow beam effect. An ideal aperture, such as the one assumed for this research, does not scatter neutrons to produce this low energy tail, and the spectrum will show no tendency to harden with depth. The present research assumed an ideal aperture, limiting the beam to those neutrons actually incident on the collimator opening. As such the present results show agreement with both of the above works. Using the results of Paretzke and co-workers, one can assume that the spectrum below 2 MeV is underestimated in the present calculations by a factor of from 10 in

Table 10. Neutron Spectra in the Heterogeneous Phantom

Detector Location	Energy Band -- Approx. Depth (cm)	9.943 - 15 MeV	4.972 - 9.943	2.486 - 4.972	1.243 - 2.486	0.621 - 1.243	0.311 - 0.621	0.155 - 0.311	0.078 - 0.155	0.039 - 0.078	0.019 - 0.039
1	0.4	1.00*	0.0021	0.0018	0.00086	0.0034	0.0018	0.0015	0.00033	0.00007	0.00067
2	3.4	0.6802	0.0028	0.0021	-	0.00022	0.0016	0.00083	0.0012	0.00093	-
3	6.4	0.5382	0.0025	0.0011	0.0020	0.00062	0.0016	0.00030	0.00090	0.00007	0.00037
4	9.5	0.4315	0.0030	0.0048	0.0015	0.00007	0.00064	0.0013	0.00015	0.00008	0.00034
5	12.5	0.3519	0.0019	0.00025	0.00020	0.0014	-	-	0.00046	0.00077	0.00013
6	15.5	0.2784	0.0013	0.00079	0.00056	0.00012	-	0.00040	-	0.00058	0.00026
7	18.6	0.2034	0.0030	0.0011	0.00014	0.00037	0.00021	0.00055	0.00087	0.0021	0.00058

*The values for all energy bands were divided by the peak value which was obtained in this band.

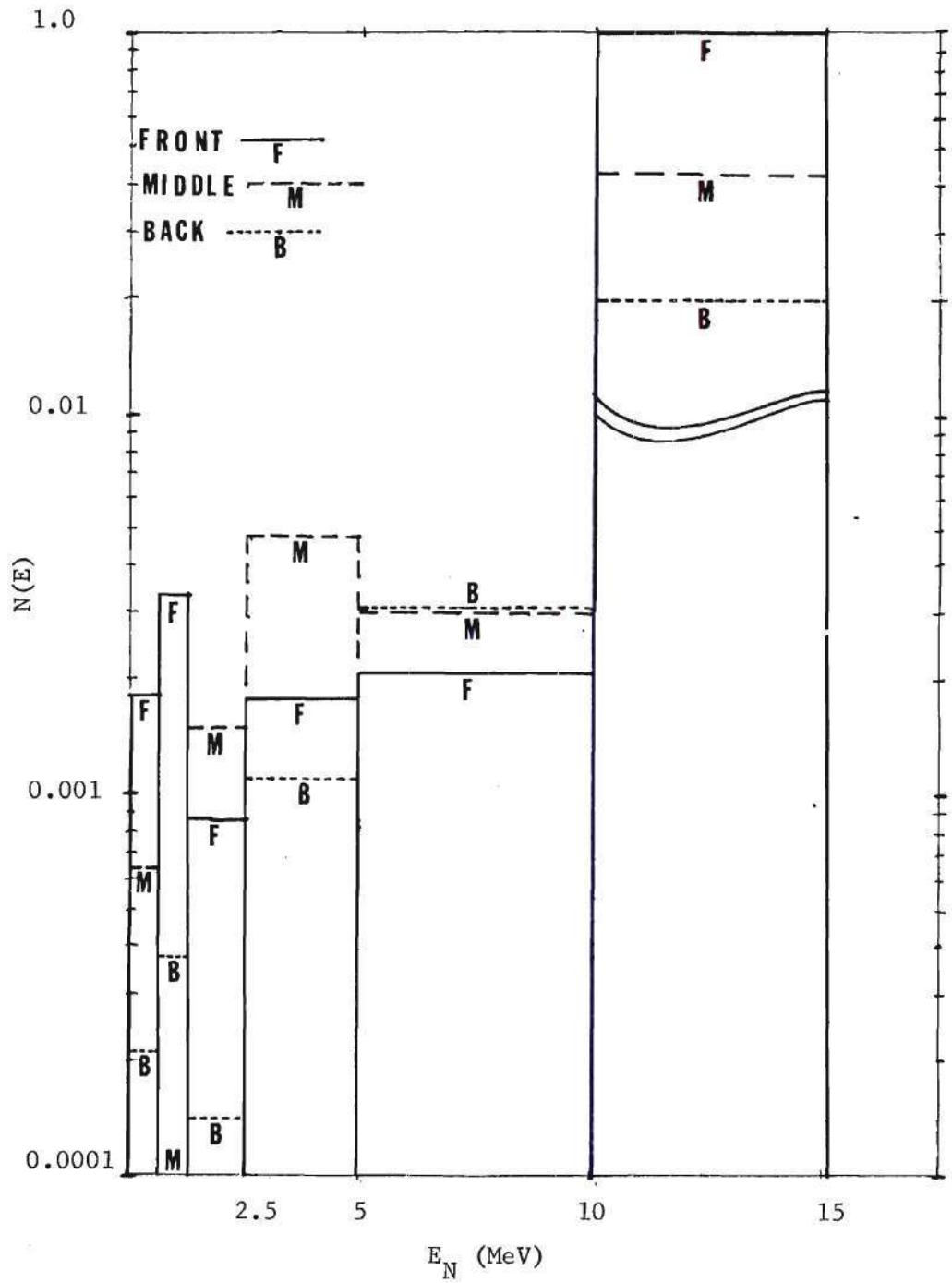

Figure 23. Calculated Neutron Spectra as a Function of Depth in the Heterogeneous Phantom with Lung, Skeleton, and Soft Tissue

the front to 2 in the rear of the phantom. As explained above, this is due to the contribution of low energy neutrons scattered in the collimator which were ignored by this calculation. Hence the low energy neutron flux plotted in Figure 23 is underestimated compared with actual conditions.

CHAPTER VI

CONCLUSIONS AND RECOMMENDATIONS

Conclusions

This research attempted to develop a code which could be used to transport neutrons and photons through a heterogeneous phantom based on Reference Man. It also attempted to test that code for 14 MeV neutrons by developing the necessary dosimetry techniques and phantom materials to simulate an actual therapy trial in Amsterdam.

From the results obtained, it is concluded that, for the most part, the Monte Carlo calculations and the measurements showed good agreement in absolute terms. Agreement with results of other investigators in similar geometries was also good. The present work demonstrated that the effects of shadowing by skeletal structures on depth dose are not greater than those of previous investigators, and may be somewhat smaller. The low neutron sensitivity of the G-M tube used to measure photon dose permitted accurate separation of the neutron and photon components of dose. This allowed the changes in depth dose due to skeletal tissue to be characterized as primarily due to photons. From plots of neutron kerma and mean free path presented in this research it is concluded that virtually no change in fast neutron dose occurs near skeletal structure; however, skeletal tissue acts as a source of photons which are produced by inelastic reaction with the skeleton.

While an inappropriate choice for the source routine resulted in

lack of complete agreement between the calculations and measurements, these results do permit one to observe that fraction of the dose in organs near a neutron beam that is due to patient scatter. Hence, these results form an estimate of organ dose under ideal conditions, and can be used to estimate the improvement that can be obtained with better collimation and shielding.

One further conclusion is that signals from small TE ion chambers can be improved with the use of unconventional TE gas mixtures. Using the TE gas based on cyclopropane that was developed for use with the TEPC in this research, an increase in signal of as much as 20% can be obtained.

Recommendations

It is recommended that the calculation of LET be separated from the transport code. The results of this calculation could be tabulated in a form that is useful to any investigator who can estimate his particular neutron spectrum. The results of Caswell and Coyne (1973) listing charged particle type and energy spectra for 13 neutron energies would provide the easiest means for calculating LET.

It is further recommended that the neutron transport code be exchanged for a current generation Monte Carlo code such as MORSE. A newer code has programming support from the various shielding centers and can use readily available cross section libraries. The fact that the adjoint problem could then be solved is another advantage of changing transport codes.

Further improvements can be made with improved source routines.

Input for these routines could be either from measured spectra at neutron therapy facilities or from Monte Carlo calculations which transport neutrons from the source through a collimator.

The largest remaining uncertainty in dosimetry after calibration is due to uncertainty in W and kerma. While improvements in kerma would be difficult to obtain without improved cross section libraries, W might be more accurately specified by estimating the charged particle spectrum, since knowledge of this spectrum would permit greater accuracy in estimating W. This estimate could be obtained from the work of Caswell and Coyne and could be used to weight W for the various charged particles. Any improvements in estimating W would result in more accurate neutron dosimetry and better inter-comparisons of fast neutron therapy trials.

BIBLIOGRAPHY

Adelson, P. H. and Kruger, P. B. (1949). "Cyclotron-induced Radiation Cataracts," Science, 110, 655.

Armstrong, T. W. and Chandler, K. C. (1973). "SPAR, A Fortran Program for Computing Stopping Powers and Ranges for Muons, Charged Pions, Protons, and Heavy Ions," Report ORNL-4869 (Oak Ridge National Laboratory, Oak Ridge, Tennessee).

Auxier, J. A., Snyder, W. S. and Jones, T. D. (1968). "Neutron Interactions and Penetration in Tissue," p. 275 in Radiation Dosimetry, Vol. I, Attix, F. H., Roesch, W. C. and Tochilin, E., Eds. (Academic Press, New York).

Auxier, J. A. (1977). "Ichiban-Radiation Dosimetry for the Survivors of the Bombings of Hiroshima and Nagasaki." Technical Information Center, U.S. Energy Research and Development Administration, Oak Ridge, Tennessee.

Bach, R. L. and Caswell, R. S. (1968). "Energy Transfer to Matter by Neutrons," Rad. Res., 35, 1.

Barkas, W. H. (1963). Nuclear Research Emulsions, Academic Press, New York, 1963, p. 438.

Barschall, H. H. and Goldberg, E. (1977). "Response of Tissue-equivalent Ionization Chamber to 15-MeV Neutrons," Medical Physics, 4, 141.

Beach, J. L. and Kelsey, C. A. (1975). "Experimentally Determined Tissue Air Ratios and Scatter Air Ratios for Collimated Beams of 14 MeV Neutrons," Int. J. Radio., 48, 134.

Benjamin, P. W., Kenshall, C. D. and Redfearn, J. (1968). "A High Resolution Spherical Proportional Counter," Nucl. Instr. Meth., 59, 77.

Bewley, D. K. (1971). "Physical Characteristics of Fast Neutron Beams," Europ. J. Cancer, 7, 99.

Bichsel, H. (1968). "Charged Particle Interactions," page 157 in Radiation Dosimetry, Vol. I, Attix, F. H., Roesch, W. C. and Tochilin, E., Eds. (Academic Press, New York).

BIBLIOGRAPHY (Continued)

Broers-Challiss, J. E., Engels, A. C., Bouts, C. J. and Broerse, J. J. (1974). "Depth Dose Measurements of D-T Neutrons in Tissue-Equivalent Phantoms," in Proc. Second Symposium on Neutron Dosimetry in Biology and Medicine, Neuherberg, Germany, EUR-5273.

Broerse, J. J., Broers-Challiss, J. E. and Maruyama, T. (1972). "Dosimetry of D-T Neutrons for Radiotherapeutic Applications," p. 627 in Proc. First Symp. Neutron Dosimetry in Biology and Medicine, Neuherberg, Germany, EUR-4896, Burger, G., Schraube, H. and Ebert, H. G., Eds. (Commission of the European Communities, Luxembourg).

Caswell, R. S. and Coyne, J. J. (1972). "Interaction of Neutrons and Secondary Charged Particles with Tissue: Secondary Particle Spectra," Rad. Res., 52, 448.

Caswell, R. S. and Coyne, J. J. (1973). "Neutron Energy Deposition Spectra Studies," p. 967 in Proc. Fourth Symp. Microdosimetry, Verbania Pallanza, Italy, EUR-5122, Booz, J., Ebert, H. G., Eickel, R. and Waker, A., Eds. (Commission of the European Communities, Luxembourg).

Catterall, M. (1971). "Clinical Experience with Fast Neutrons from the Medical Research Council's Cyclotron at Hammersmith Hospital," Eur. J. Cancer, 7, 227.

Catterall, M. (1974). "The Treatment of Advanced Cancer by Fast Neutrons from the Medical Research Council's Cyclotron at Hammersmith Hospital, London, Eur. J. Cancer, 10, 343.

Chen, W. L., Shinpaugh, W. H., Hubbell, H. H. and Poston, J. W. (1971). "Dose Distributions from Neutrons Incident on a Tissue-Equivalent Phantom," ORNL-TM-3425, Thesis, University of Tennessee.

Colvett, R. D. (1974). "Neutron Dose Response of a Geiger-Mueller Counter," p. 152 in Annual Report on Research Project, USAEC Report COO-3243-3 (National Technical Information Service, U.S. Department of Commerce, Springfield, Virginia).

Evaluated Nuclear Data File (ENDF/B). (1975). Version IV available from National Neutron Cross Section Center, Brookhaven National Laboratory, Upton, New York.

Failla, G. (1937). "The Measurement of Tissue Dose in Terms of the Same Unit for All Ionizing Radiations," Radiology, 29, 202-215.

Fitzgerald, J. J., Brownell, G. L. and Mahoney, F. J. (1967). Mathematical Theory of Radiation Dosimetry, Gordon and Breach, New York, p. 440.

BIBLIOGRAPHY (Continued)

Fowler, J. F. and Morgan, R. L. (1963). "General Review of: Pre-therapeutic Experiments with the Fast Neutron Beam from the Medical Research Council's Cyclotron," British J. Radiol., 36, 77.

Fowler, J. F. (1964). "Neutrons in Radiotherapy," in Biological Effects of Neutron and Proton Irradiations," I.A.E.A., Vienna, Vol. II, p. 185.

Fry, R. J. M., Gregg, E. C., Painter, R. B. and Roesch, W. C. (1972). "High-LET Radiation in Radiotherapy," Radiology, 103, 215.

Garry, S. M., Stansbury, P. S. and Poston, J. W. (1974). "Measurement of Absorbed Fractions for Photon Sources Distributed Uniformly in Various Organs of a Heterogeneous Phantom," ORNL-TM-4411 (Oak Ridge National Laboratory, Oak Ridge, Tennessee).

Greene, D. and Thomas, R. L. (1968). "An Experimental Unit for Fast Neutron Radiotherapy," Brit. J. Radiol., 41, 455.

Goldstein, H. (1959). Fundamental Aspects of Reactor Shielding, Addison-Wesley Co., Cambridge, Massachusetts.

Goodman, L. J. (1974). "Problems in Neutron Dosimetry," Eur. J. Cancer, 10, 309.

Hurst, G. S. (1954). "An Absolute Tissue Dosimeter for Fast Neutrons," Brit. J. Radiol., 27, 353.

ICRP. (1975). International Commission on Radiological Protection, Report of Task Group on Reference Man, ICRP Report 23 (Pergamon Press, New York).

ICRU. (1977). International Commission on Radiation Units and Measurements, Neutron Dosimetry for Biology and Medicine, ICRU Report 26, Washington, D. C.

Irving, D. C. Freestone, R. M. and Kam, F. B. K. (1965). "05R, A General-Purpose Monte Carlo Neutron Transport Code," ORNL-3622 (Oak Ridge National Laboratory, Oak Ridge, Tennessee).

Jones, T. D., Snyder, W. S. and Auxier, J. A. (1971). "Absorbed Dose, Dose Equivalent, and LET Distributions in Cylindrical Phantoms Irradiated by a Collimated Beam of Monoenergetic Neutrons," Health Physics, 21, 253.

Lewis, V. E. and Young, D. J. (1977). "Measurement of the Fast Neutron Sensitivities of Geiger-Mueller Counter Gamma Dosimeters," Physics in Med. and Biol., 22, 476.

BIBLIOGRAPHY (Continued)

Lindhard, J., Scharff, M. and Schiott, H. E. (1963). "Range Concepts and Heavy Ion Ranges," Mat. Fys. Medd. Dan. Vid. Selsk., 33, No. 14.

Marshall, J. H., Lari, R. J. and Kastner, J. (1964). "Diffusion and Absorption of Gases in Plastic-walled Ionization Chambers," Health Physics, 10, 331.

Mays, C. (1977). Private Communication to T. D. Jones, Oak Ridge National Laboratory, Oak Ridge, Tennessee.

McGinley, P. H. (1973). "Depth Dose Distributions Due to 14 MeV Neutrons," Health Phys., 25, 191.

McGinley, P. H. (1971). "Fast Neutron Therapy Treatment Planning," Dissertation, Georgia Institute of Technology, Atlanta, Georgia.

McGinley, P. H. and McLaren, J. R. (1976). "Distortion of Fast-neutron Dose Distribution by Bone," Medical Physics, 3, 181.

McGinley, P. H. and McLaren, J. R. (1974). "Perturbation of Neutron Dose Distribution by Lung Tissue," Medical Physics, 1, 219.

Mijnheer, B. J., Broers-Challiss, J. E. and Broerse, J. J. (1975). "Measurements of Radiation Components in a Phantom for a Collimated D-T Neutron Beam," p. 423 in Proc. Second Symp. Neutron Dosimetry in Biology and Medicine, Neuherberg, Germany, EUR-5273, Burger, G. and Ebert, H. G., Eds. (Commission of the European Communities, Luxembourg).

NBS. (1964). National Bureau of Standards, "Physical Aspects of Irradiations," NBS Handbook 85, Washington, D. C.

NPL. (1973). National Physical Laboratory," Dosimetry Practice in Neutron Radiotherapy Centres in Great Britain," NPL Report RS 1, London, United Kingdom.

Paretzke, H. G., Grünauer, F., Maier, E. and Burger, G. (1972). "The Change of Radiation Quality in a Neutron Irradiated Phantom," p. 73 in First Symp. on Neutron Dosimetry in Biology and Medicine, Neuherberg, Germany, EUR-4896d-f-e.

Penney, S. K., Trubey, D. K. and Emmett, M. B. (1963). "OGRE, A Monte Carlo System for the Study of Gamma Ray Transport; with an Example," ORNL-3805, (Oak Ridge National Laboratory, Oak Ridge, Tennessee).

Poston, J. W. (1971). "Neutron Depth Dose Distributions in Heterogeneous Phantoms," ORNL-TM-3329; Dissertation, Georgia Institute of Technology, Atlanta, Georgia.

BIBLIOGRAPHY (Continued)

Powers, W. E. (1972). "Introduction to the Conference on Particle Accelerators in Radiation Therapy, LA-5180-C, 1, Los Alamos, New Mexico.

Ritts, J. J., Solomito, M. and Stevens, P. N. (1970). "The Calculation of Neutron-Induced Physical Doses in Human Tissues," ORNL-2991 (Oak Ridge National Laboratory, Oak Ridge, Tennessee).

Rossi, H. H. and Rosenzweig, W. (1955). "A Device for the Measurement of Dose as a Function of Specific Ionization," Radiology, 64, 404.

Rossi, H. H. (1968). "Microscopic Energy Distribution in Irradiated Matter," p. 43 in Radiation Dosimetry, Vol. I, Attix, F. H., Roesch, W. C. and Tochilin, E., Eds. (Academic Press, New York).

Shonka, J. J. and McGinley, P. H. (1976). "Preparation of Phantom Lung Material," Health Physics, 21, 150.

Shonka, J. J., Gritzinger, C. M. and Poston, J. W. (1975). "Some Operating Characteristics of Tissue-Equivalent Proportional Counter," p. 254, ORNL-5046 (Oak Ridge National Laboratory, Oak Ridge Tennessee).

Smathers, J. B., Otte, V. A., Smith, A. R., Almond, P. R., Attix, F. H., Spokas, J. J., Quam, W. M. and Goodman, L. J. (1977). "Composition of A-150 Tissue-Equivalent Plastic," Medical Physics, 4, 74.

Smith, A. R., Almond, P. R., Smathers , J. B., Otte, V. A., Attix, F. H., Theus, R. B., Wootton, P., Bichsel, H., Eenmaa, J., Williams, D., Bewley, D. K. and Parnell, C. J. (1975). "Dosimetry Intercomparisons Between Fast-neutron Radiotherapy Facilities," Medical Physics, 2, 195.

Snyder, W. S. and Neufeld, J. (1955). "Calculated Depth Dose Curves in Tissue for Broad Beams of Fast Neutrons," Brit. J. Radiol., XXVIII, 342.

Snyder, W. S. (1964). "The LET Distribution of Dose in Some Tissue Cylinders," p. 3, in Biological Effects of Neutron and Proton Irradiations, Vol. I, IAEA, Vienna.

Snyder, W. S., Fisher, H. L., Ford, M. R. and Warner, G. G. (1968). "Mathematical Description of the Body Organs," J. Nucl. Med. Suppl. 3, Pamphlet 5, Appendix B, 46.

Srdoc, D. (1970). "Experimental Technique of Measurement of Microscopic Energy Distribution in Irradiated Matter Using Rossi Counters," Rad. Res., 43, 302.

BIBLIOGRAPHY (Continued)

Stone, R. S. and Larkin, J. C. (1942). "Treatment of Cancer with Fast Neutrons," Radiology, 39, 608.

Stone, R. S. (1948). "Neutron Therapy and Specific Ionization," Am. J. Roentgen, 59, 771.

Straker, E. A., Stevens, P. N., Irving, D. C. and Cain, V. R. (1970). "The MORSE Code, a Multigroup Neutron and Gamma-Ray Monte Carlo Transport Code," ORNL-4585 (Oak Ridge National Laboratory, Oak Ridge, Tennessee).

Suit, H. D. (1969). "Statement of the Problem Pertaining to the Effect of Dose Fractionation and Total Treatment Time on Response of Tissue to X-Irradiation," BNL-50203 (C-57), vii (Brookhaven National Laboratory

Thorngate, J. H. and Johnson, D. R. (1965). "The Response of a Neutron-insensitive Gamma-ray Dosimeter as a Function of Photon Energy," Health Phys., 11, 133.

Theus, R. B., Bondelid, R. O., Attix, F. H., August, L. S., Shapiro, P., Surratt, R. E. and Rogers, C. C. (1974). "Physical Characteristics of the NRL Fast Neutron Beam for Radiation Therapy," Cancer, 34, 17.

Van Peperzeel, H. A., Breur, K., Broerse, J. J. and Barendsen, G. W. (1974). "RBE Values of 15 MeV Neutrons for Responses of Pulmonary Metastases in Patients," Eur. J. Cancer, 10, 349.

Victoreen Instrument Division, 10101 Woodland Avenue, Cleveland, Ohio 44104

Wagner, E. B. and Hurst, G. S. (1959). "Gamma Response and Energy Losses in the Absolute Fast Neutron Dosimeter," Health Physics, 2, 57.

Wagner, E. B. and Hurst, G. S. (1961). "A Geiger-Mueller γ-Ray Dosimeter with Low Neutron Sensitivity," Health Physics, 5, 20.

Warner, G. G. and Craig, A. M. (1968). "Algam, A Computer Program for Estimating Internal Dose from Gamma-Ray Sources in a Man Phantom," ORNL-TM-2250 (Oak Ridge National Laboratory, Oak Ridge, Tennessee).

Wilkie, W. H. (1971). "Theoretical Image-forming Quality of Fast Neutron Radiography," Dissertation, Georgia Institute of Technology, Atlanta, Georgia.

Williamson, F. S. and Mitacek, P., Jr. (1967). "Calculations of Kerma Due to Fast Neutrons in Tissue-Like Materials," in Neutron Monitoring, 17-26, IAEA, Vienna.

VITA

Joseph John Shonka was born in Chicago, Illinois. He received the B.S. Degree in Physics from St. Procopius College in 1969 and the M.S. Degree in Physics from Georgia Institute of Technology in 1970.

Mr. Shonka's Master's degree was funded by a fellowship from the United States Public Health Service, and his doctoral research was performed at the Oak Ridge National Laboratory under a Laboratory Fellowship administered by Oak Ridge Associated Universities. Mr. Shonka's specialization is Medical Physics, and his publications include:

"A Comparison of the GTC Cross Sections with ENDF/BIII," (1974) in the Annual Progress Report of the Health Physics Division for the period ending July 31, 1974. Report ORNL-4979 (with T. D. Jones)

"Some Operating Characteristics of Tissue-Equivalent Proportional Counters," (1975) p. 254 in the Annual Progress Report of the Health Physics Division for the period ending June 30, 1975. Report ORNL-5046 (with others)

"Progress Report on the Reference Man Code, RMC," (1976) p. 84 in the Annual Progress Report of the Health Physics Division Annual Progress Report for the period ending June 30, 1976. Report ORNL-5171

"Preparation of Phantom Lung Material," (1976) Physics in Medicine and Biology. 21, p. 150 (with P. H. McGinley)

Mr. Shonka is an associate or student member of the American Nuclear Society, the Health Physics Society, The American Association of Physicists in Medicine and Sigma Xi. He is married to the former Deborah F. Burch of Beaufort, South Carolina.